Nucleic Acids Research, 2025, **53**, gkaf088
https://doi.org/10.1093/nar/gkaf088
Gene regulation, Chromatin and Epigenetics

RNA exosome-driven RNA processing instructs the duration of the unfolded protein response

Laura Matabishi-Bibi[1], Coralie Goncalves[2], Anna Babour[1,2,*]

[1]Université Paris Cité, INSERM U944 and CNRS 7212, Institut de Recherche Saint Louis, Hôpital Saint Louis, 75475 Paris Cedex 10, France
[2]Université Paris Cité, CNRS 7592, Institut Jacques Monod, F-75013 Paris, France
[*]To whom correspondence should be addressed. Email: anna.babour@ijm.fr

Abstract

Upon stresses, cellular compartments initiate adaptive programs meant to restore homeostasis. Dedicated to the resolution of transient perturbations, these pathways are typically maintained at a basal level, activated upon stress, and critically downregulated upon reestablishment of cellular homeostasis. As such, prolonged activation of the unfolded protein response (UPR), a conserved adaptive transcriptional response to defective endoplasmic reticulum (ER) proteostasis, leads to cell death. Here, we elucidate an unanticipated role for the nuclear RNA exosome, an evolutionarily conserved ribonuclease complex that processes multiple classes of RNAs, in the control of UPR duration. Remarkably, the inactivation of Rrp6, an exclusively nuclear catalytic subunit of the RNA exosome, curtails UPR signaling, which is sufficient to promote the cell's resistance to ER stress. Mechanistically, accumulation of unprocessed RNA species diverts the processing machinery that maturates the messenger RNA encoding the master UPR regulator Hac1, thus restricting the UPR. Significantly, Rrp6 expression is naturally dampened upon ER stress, thereby participating in homeostatic UPR deactivation.

Graphical abstract

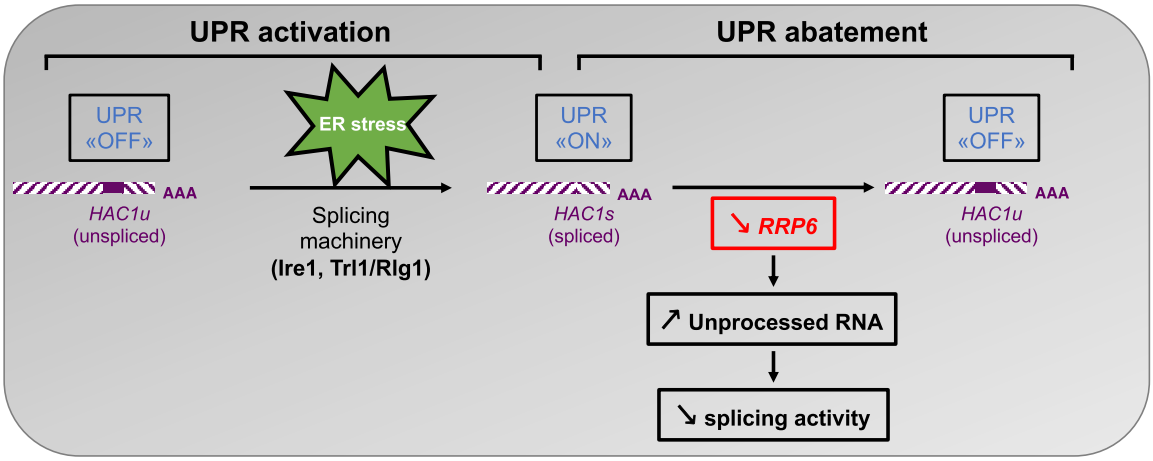

Introduction

Multiple perturbations of the intracellular or extracellular microenvironment can disturb cellular homeostasis. To cope with these various stresses, cells activate specific molecular mechanisms and adaptive responses. In this way, endoplasmic reticulum (ER) stress—defined as the intra-luminal accumulation of unfolded proteins set off by a disruption of ER homeostasis—triggers an adaptive signaling pathway named the unfolded protein response (UPR). Hence, the UPR is a transcriptional signaling pathway conserved from yeast to humans, which drives an expression program designed to survive conditions that alter the proteostasis of the ER, defined as ER stress [1].

In *Saccharomyces cerevisiae*, the UPR is set in motion by a unique ER-associated kinase and ribonuclease inositol-requiring protein 1, Ire1 (IRE1αβ in metazoans). Upon ER stress, Ire1 oligomerization and trans-autophosphorylation allow self-activation and severing of a 252-nucleotides translation inhibitory intron in the constitutively expressed messenger RNA (mRNA) of a basic leucine zipper transcription factor, Hac1 (XBP1 in metazoans). A stem-loop located in the 3′-untranslated region (3′UTR) of the *HAC1* mRNA and named

Received: October 31, 2024. **Revised:** January 27, 2025. **Editorial Decision:** January 29, 2025. **Accepted:** February 3, 2025

3′-BE (3′ Bipartite Element), targets *HAC1* mRNA to Ire1 foci in the ER membrane to ensure rapid Ire1-mediated cleavage following ER stress [2]. This conserved unconventional cytoplasmic splicing event is completed by the transfer RNA (tRNA) ligase Trl1/Rlg1 [3] (RTCB complex in mammals), which joins *HAC1* exons, thus resuming the block in translation initiation imposed by a secondary structure in the 3′ UTR of *HAC1* mRNA [4–6]. In turn, Hac1 expression culminates in the transcriptional activation of effectors that attenuate ER stress and restore the biosynthetic ability of the ER [7].

Importantly, kinetics analysis, using chemical inducers of ER stress in mammalian and yeast cells, revealed the transience of Ire1-mediated UPR signaling, despite the persistence of the inducer [8, 9]. As such, although the UPR homeostatically matches the ER protein-folding capacity to cellular needs, it triggers apoptosis in mammals under high or chronic ER stress [10]. Similarly, failure to dampen the UPR compromises yeast cell viability despite normal initial UPR transcriptional activation [8, 11, 12], likely due to massive overloading of the ER translocation machinery [11–13]. While the causal relationship between prolonged UPR and loss of cell viability is counterintuitive due to the protective nature of UPR, it is, nonetheless, reminiscent of the yeast heat shock response, whose deactivation is tightly regulated to maximize cellular fitness [14, 15] and of the mitochondrial UPR whose constitutive activation decreases the lifespan of *Caenorhabditis elegans* [16]. The significance of UPR abatement for the fate of cells experiencing ER stress is further emphasized by the diversity of reported mechanisms for UPR deactivation [11, 17–22]. In this regard, we recently revealed a novel mechanism, driven by the nuclear retention of the *HAC1* transcript via a direct interaction between its 3′UTR and the chromatin remodeler [23] and mRNA quality control factor [24, 25], Isw1. In addition, Isw1 being itself ER stress-induced, we proposed that the restriction it imposes on *HAC1* mRNA nuclear export allows the timely deactivation of the UPR, thus ensuring homeostatic adaptation to ER stress [12].

Since Isw1 exerts its nuclear mRNA quality control activity in cooperation with the exclusively nuclear catalytic subunit of the RNA exosome Rrp6 (EXOSC10) [25], we were prompted to explore whether Rrp6 activity would also contribute to UPR regulation. The RNA exosome is a multisubunit complex that cooperates with dedicated co-factors to monitor virtually every class of transcripts [26, 27], including pre-ribosomal RNA (rRNA) processing and tRNA maturation [28, 29]. The inactivation of *RRP6* was previously reported to increase cells' resistance to ER stress [30, 31], in striking contrast with the inactivation of *ISW1,* which increases cells' sensitivity to ER stress [12]. This resistance to ER stress was associated with a stabilization of the mRNA encoding the UPR transcription factor Hac1 as well as an ER stress-mediated reduction of Rrp6 expression. In this context, a model was suggested, in which the timely degradation of the unspliced form of *HAC1* would allow accurate UPR activation and deactivation, both essential to ER stress survival. This model posits that under basal conditions, the exonucleolytic activity of Rrp6 would allow the formation of a pool of 'nonspliceable' forms of *HAC1* mRNA that lack the 3′BE element, thus favoring post-transcriptional silencing. As such, the increased resistance of *rrp6*Δ cells would stem from enhanced UPR signaling resulting from the splicing of an increased pool of 3′BE-containing *HAC1* mRNA molecules [31].

Unexpectedly, we report here that *rrp6*Δ cells' resistance to ER stress goes along with faster UPR shutdown and demonstrate that the mere shortening of UPR signaling duration is sufficient to confer ER stress resistance. Mechanistically, the inactivation of *RRP6* impedes *HAC1* mRNA splicing through the accumulation of unprocessed RNA species, which titrate *HAC1* splicing machinery, thereby limiting UPR activation. Remarkably, the physiological ER stress-induced downregulation of *RRP6* expression restrains *HAC1* mRNA splicing, allowing timely attenuation of UPR signaling and homeostatic adaptation to the stress.

Materials and methods

Yeast strains, growth conditions

The *S. cerevisiae* strains used in this study are described in Table 1. Cells were grown in YPD medium (1% yeast extract, 2% bactopeptone, and 2% glucose) or dropout base supplemented with the appropriate CSM-aminoacid (MP Biomedicals, LCC) media, at 30°C unless otherwise noted. To induce ER stress in liquid cultures, yeast cells were treated with 2 mM of dithiothreitol (DTT; VWR) or 1 μg/ml of tunicamycin (Tm; Sigma). Gene deletions and tagging were created by one-step polymerase chain reaction (PCR) mediated strategy, as described in [32]. The *IRE1-AID* strain was built by insertion of plasmids pRS305-*IRE1-AID-HA* into *leu2-3 112* after linearization by AflII and pOs-TIR1 into *ura3-1* after StuI linearization. The *RRP6-AID* strain was constructed by homologous recombination as in [32], by transformation of W303 wild type strain with the PCR products obtained by amplification of plasmid pMK43 with primers DL4474 and DL3567 and plasmid Addgene 102 883 [33] with primers DL3568 and DL4475. Strains used in this study are listed in Table 1.

Plasmids

All plasmids were built using standard PCR-based molecular cloning techniques and are listed in Table 2.

For plasmid pRS305-*IRE1-AID-HA,* an AID-3HA module was inserted after the transmembrane domain of Ire1 by assembling PCR products amplified from genomic DNA with primers AB584/AB585 and AB588/AB589 and from plasmid pHyg-AID*-6HA with primers AB586/587 into ApaI/SacI-digested pRS305 plasmid. Plasmid pRS314-$_{ADH}$*IRE1* was obtained by replacing *IRE1* endogenous promoter with the *ADH* promoter in XhoI linearized plasmid pCS110 [34], by amplifying the *ADH* promotor on plasmid p414-ADH with primers AB519/AB520. Plasmid p$_{PMI40}$-*RRP6* resulted from the assembly of the following PCR products amplified with AB680/AB681 and AB682/AB701 on genomic DNA and pAC1981, respectively, into EcoRI/BamHI digested pRS316 plasmid. All primers used in this study are described in Table 3. All plasmids were verified by Sanger sequencing.

Plate-based growth assays

Growth assays were performed by spotting serial dilutions of exponentially growing cells on solid medium with a Replica plater and incubating the plates at the indicated temperatures for 2–3 days. When indicated, Tm was added to the growth medium at concentrations ranging from 0.2 to 0.8 μg/ml. Control plates (−ER stress) contained 4 μl of dimethylsulfoxyde (DMSO, drug carrier). Each growth assay is a representative example of at least three biological replicates. DTT sensitivity plate assay was performed upon incubation of the plates in an anaerobic chamber, using Anaerocult® A (Merck) for the production of an anaerobic milieu.

Table 1. Yeast strains used in this study

Name	Genotype	Origin
W303	*Mat α leu2-3 112 trp1-1 can1-100 ura3-1 ade2-1 his3-11,15*	Lab collection
rrp6Δ	*Mat a leu2-3 112 trp1-1 can1-100 ura3-1 ade2-1 his3-11,15, rrp6 ::KanMx*	Lab collection
ire1Δ	*Matα leu2-3 112 trp1-1 can1-100 ura3-1 ade2-1 his3-11,15, ire1::HPH*	Lab collection
RRP6-AID	*Mat a leu2-3 112 trp1-1 can1-100 ura3-1 ade2-1 his3-11,15, RRP6::AID::KanMx::OsTIR1*	This study
lrp1Δ	*Matα leu2-3 112 trp1-1 can1-100 ura3-1 ade2-1 his3-11,15, lrp1:: KanMx*	This study
trf4Δ	*Matα leu2-3 112 trp1-1 can1-100 ura3-1 ade2-1 his3-11,15, trf4:: KanMx*	Lab collection
DIS3	*Mat a leu2-3 112 trp1-1 can1-100 ura3-1 ade2-1 his3-11,15, DIS3 ::KanMx [pBS3269-DIS3-TEV-ProtA,LEU2]*	D. Libri [29]
dis3 endo-	*Mat a leu2-3 112 trp1-1 can1-100 ura3-1 ade2-1 his3-11,15, DIS3 ::KanMx [pBS3269-dis3D171N-TEV-ProtA,LEU2]*	D. Libri [29]
DIS3	*Mat a leu2-3 112 trp1Δ can1-100 ura3-1 ade2-1 his3-11,15, KanMx:TetOFF-DIS3 [pBS3269-DIS3-TEV-ProtA,LEU2]*	D. Libri [43]
dis3 exo-	*Mat a leu2-3 112 trp1Δ can1-100 ura3-1 ade2-1 his3-11,15, KanMx:TetOFF-DIS3 [pBS3269-dis3D551N-TEV-ProtA,LEU2]*	D. Libri [43]
dis3 endo-exo-	*Mat a leu2-3 112 trp1Δ can1-100 ura3-1 ade2-1 his3-11,15, KanMx:TetOFF-DIS3 [pBS3269-dis3D551N-D171N-TEV-ProtA,LEU2]*	D. Libri [43]
xrn1Δ	*Matα leu2-3 112 trp1-1 can1-100 ura3-1 ade2-1 his3-11,15, xrn1:: KanMx*	Lab collection
upf1Δ	*Matα leu2-3 112 trp1-1 can1-100 ura3-1 ade2-1 his3-11,15, upf1:: KanMx*	Lab collection
deg1Δ	*Matα leu2-3 112 trp1-1 can1-100 ura3-1 ade2-1 his3-11,15, deg1:: KanMx*	This study
los1Δ	*Matα leu2-3 112 trp1-1 can1-100 ura3-1 ade2-1 his3-11,15, los1:: KanMx*	This study
nmd2Δ	*Matα leu2-3 112 trp1-1 can1-100 ura3-1 ade2-1 his3-11,15, nmd2:: KanMx*	This study
IRE1-AID	*Matα leu2-3 112*:: pRS305-*IRE1*-AID-HA, *trp1-1 can1-100 ura3-1*:: pNHK53-Os *TIR1, ade2-1 his3-11,15, ire1::HPH*	This study
SEN2	Mata *leu2-3 112 trp1-1 can1-100 ura3-1 ade2-1 his3-11,15*	A. Hopper(35)
sen2-42	Mata *leu2-3 112 trp1-1 can1-100 ura3-1 ade2-1 his3-11,15 sen2 ::leu2Δ :HPH/ptySC262 (sen2-42 <TRP>)*	A. Hopper(35)
isw1Δ	*Matα leu2-3 112 trp1-1 can1-100 ura3-1 ade2-1 his3-11,15, isw1::KanMx*	Lab collection
rrp6Δisw1Δ	*Matα leu2-3 112 trp1-1 can1-100 ura3-1 ade2-1 his3-11,15, rrp6 ::KanMx, isw1::HPH*	This study
hac1Δ	*Matα leu2-3 112 trp1-1 can1-100 ura3-1 ade2-1 his3-11,15, hac1::HPH*	Lab collection
maf1Δ	*Mat a leu2-3 112 trp1-1 can1-100 ura3-1 ade2-1 his3-11,15, maf1 ::KanMx*	This study

Table 2. Plasmids used in this study

Plasmid name	Origin
p414-ADH	Lab collection (ATCC 87372™)
pCS110	Lab collection [34]
pRS316-*RRP6*	Lab Collection
pRS316-*rrp6D238A*	Lab Collection
pRS314-$_{ADH}$*IRE1*	This study
pMK43	Lab collection [33]
p_{ADH} Os*TIR1*	Addgene 102 883
pOs*TIR1*	Lab collection (pNHK53 [74]
pHyg-AID*-6HA	Lab collection [74]
pRS305-*IRE1-AID-HA*	This study
p_{CUP}-*RLG1*-FL	T. Yoshihisa (pTYSC463)
pRS316-*HAC1*	M. Dey
pRS316-*hacΔi*	M. Dey
pRS415$_{ADH}$-*ISW1-2FL*	Lab collection
P_{PMI40}-*RRP6*	This study

Viability assays

For viability assays, cells were stained with 5 μg/ml propidium iodide (PI; Sigma, 1 mg/ml in water) for 20 min in the dark at room temperature. PI fluorescence was examined from at least 400 cells in three biological replicates under a fluorescence microscope and red fluorescent cells (dead) were counted.

RNA extraction

Total RNAs were purified from 10 optical density 600 nm (OD_{600}) of snap frozen cells using the Nucleospin RNAII kit (Macherey Nagel) according to the manufacturer's instructions. RNA integrity was verified by gel electrophoresis. Samples were aliquoted and snap frozen at −80°C or directly further processed. For reverse transcription quantitative polymerase chain reaction (RT-qPCR), 300 ng of NanoDrop™ One-quantified RNA were reverse-transcribed using random hexamers [P(dN)6, Roche] and Superscript II reverse transcriptase (Thermo Fisher Scientific) according to the manufacturer's recommendations in a 20 μl final volume.

Complementary DNA samples analysis

Complementary DNA (cDNA) was quantified by qPCR in accordance with MIQE guidelines using the Master Mix PCR Power SYBR™ Green (Thermo Fisher). Ten microliter reactions containing a 1/40 dilution of 300 ng reversed-transcribed RNA were prepared according to the manufacturer's instructions, dispensed into a 96-well plate with an epMotion® 5070 (Eppendorf), and analyzed with a QuantStudio5™ apparatus (Applied Biosystems™).The following qPCR cycles were performed: following an initial denaturation at 95°C for 5 min, amplification occurred during 45 cycles of denaturation (95°C for 15 s) and annealing/extension (60°C for 50 min) with fluorescence measurements taken each cycle. The resulting Cq values were analyzed via the Standard Curve module of the Applied Biosystems™ Analysis Software, which measures amplification of the target in samples and in a standard dilution series. Extraneous nucleic acid contamination and DNA contamination were controlled via the systematic inclusion of no template and no reverse transcriptase controls. Reactions specificities were controlled by melting curves analysis (slow ramp to 95°C, 0.05°C/s). qPCR primers were designed with Primer3web version 4.1.0 (Tm 60°C, amplicon ≈ 150 bp) and are listed in Table 3 as qABxx. Primers were purchased desalted from Eurofins Genomics. Samples were run in triplicate. qPCR validation parameters are presented in Table 4. The number of biological replicates is indicated in the figure legends. Analysis of *HAC1* mRNA splicing was performed as previously described [12] with primers specific for the unspliced (qAB88/qAB91), spliced (qAB91/qAB135), and total (qAB124/qAB125) forms of *HAC1*.

Deep sequencing

mRNA sequencing libraries were prepared and sequenced with Illumina technology by Novogene (Novogene Co., Ltd) from polyA + RNAs purified from 1 μg of total RNA using NEBNext® UltraTM RNA Library Prep Kit for Illumina® (NEB, USA) following the manufacturer's recommendations and index codes were added to attribute sequences to each sample. Briefly, mRNA was purified from total RNA using poly-T oligo-attached magnetic beads. Fragmentation was

Table 3. Primers used in this study

Primer	Target	Primer sequence
AB519	*ADH* promoter	F, ATTAACCCTCACTAAAGGGAACAAAAGCTGGGTACCGGGCCCCCCCTCGAATCCTTTTGTTGTTTCCGGGTG
DL4474	*AID*	GAGGAGGCCTGCCGCCAAAGGTAAGAATCTGTCATTTAAAAGGCGTACGCTGCAGGTCGAC
DL3567	*AID*	ATCCTGGTATCGGTCTGCG
DL3568	*TIR1*	AATGTCGGGCTAATCAGG
DL4475	*TIR1*	ATGAAAATTACCATAATTTATAAATAAAAAAATACGCTTGTTTTACATAAGGAAACAGCTATGACCATG
AB520	*ADH* promoter	R, ACACAAACGAGCAGTGTCAATACTAACATGTTTCTTCGAAGTAGACGCATAGTTGATTGTATGCTTGGTATAGCTT
AB584	*IRE1*	F, TATCCCTATGACGTCCCGGACTATGCAGGATCCTATCCATATGACGTTCCAGATTACGCTGGATTTATGCCTGAAAAGGAAATCCC
AB585	*IRE1*	R, ACCATGATTACGCCAAGCTCGGAATTAACCCTCACTAAAGGGAACAAAAGCTGGGTACCGAGCTTTCCACCAAAAAAGTCAGTG
AB586	*AID*	F, GTGCAATACTACAAAGATTCAAAATTTTGCCGCCACTATATGTATTATTATCCAAAATTGCCTAAAGATCCAGCCAAACCTCC
AB587	*AID*	R, AAGAGGGACAATTTAGCGATTTCGACTCAACTATGGGGATTTCCTTTTCAGGCATAAATCGCGTAATCTGGAACGTCATATGGATA
AB588	*IRE1*	F, ACGTTGTAAAACGACGGCCAGTGAATTGTAATACGACTCACTATAGGGCGAATTGGAGCTTGGGCTTTTAGGGACAGTTCTATTCTTC
AB589	*IRE1*	R, CTCACCGGTGGCCATCCCACAACTTGTGCCTTGGCCGGAGGTTTGGCTGGATCTTTAGGAATTTTGGATAATAATACATATAGTGGCGGC
AB680	*PMI40* promoter	F, CGGCCGCTCTAGAACTAGTGCCACAACTTTATCAGTGG
AB681	*PMI40* promoter	R, CAGAAGTCATGTTTTAAAATTTTCTGGTCTGATG
AB682	*RRP6*	F, ATTTTAAAACATGACTTCTGAAAATCCG
AB701	*RRP6*	R,TATCGATAAGCTTGATATCGTCACCTTTTAAATGACAGATTC
qAB88	*HAC1*u	R, CATCGTAATCACGGCTGGA
qAB91	*HAC1*u/s	F, CCTGCCGTAGACAACAACAA
qAB135	*HAC1*s	R, TCAAACCTGACTGCGCTTCT
qAB124	*HAC1* Tot	F, TACGTTCACACCTTCACCTCTG
qAB125	*HAC1* Tot	R, TCCGTCTTAAACATCTGCAGCT
qAB114	*IRE1*	F, ATTTCGGGAGCCAGAGTGTG
qAB115	*IRE1*	R, TGAAGCGCTAGGGGAACATC
qAB140	*RLG1*	F, TGGCAAAACAACAACTTCCCAG
qAB141	*RLG1*	R, CGCGGAATTGGTGATTGTTTCT
qAB98	*SCR1*	F, GTTCTGAAGTGTCCCGGCTATAA
qAB99	*SCR1*	R, CACCAGACAGAGAGACGGATTC
qAB8	*18S*	F, ATCTTGTGAAACTCCGTCGTG
qAB9	*18S*	R, CAAATTCTCCGCTCTGAGATG
qAB140	*RLG1*	F, TGGCAAAACAACAACTTCCCAG
qAB148	*tLEU(CAA)*	F, GGTTGTTTGGCCGAGCGGTCTAAG
qAB150	*tLEU(CAA)*	R, TATTCCCACAGTTAACTGCGGTC
qAB116	*RRP6*	F, CGCCACGATTTGTTATGCCA
qAB117	*RRP6*	R, TCTGGCGGACATGTTCAGTT
AB350	*HAC1*	R, AGCGTGGCTCTTTGAGGT
AB357	*HAC1*	F, AAGAAGAAGAGGCTTTTCAAGAATGC
qAB246	*snR37*	F, GTGAGTGATGAGGAGCTTGC
qAB247	*snR37*	R, GAAACCGGAAACGAAATGAAAATTGTTAC
qAB248	*snR37*-ETs	F, TTTGTATACTTTCTCATTCCCATAATTTGTAGTGC
qAB249	*snR37*-ETs	R, ATCTCGATATACGCACCGTACACG

Table 4. qPCR validation parameters

	Efficiency (%)	Slope of standard curve	y-intercept	R-squared	Cq + RT	Cq noRT	Cq NTC
HAC1u qAB88/91	86.00–93.15	−3.7 to −3.49	24.67–27.81	0.97–0.98	17.51–19.13	29.13–29.96	30.32–30.48
HAC1s qAB91/135	89.64–94.21	−3.46 to −3.59	24.53–24.70	0.96–0.98	17.23–18.78	30.79–30.60	31.25–31.49
HAC1Tot qAB124/125	97.83–97.94	−3.3748 to −3.37	24.00–27.81	0.99–0.99	16.71–20.59	27.88–30.17	30.40–31.64
IRE1 qAB114/115	99.16–101.71	−2.9595 to −2.52	22.15–23.11	0.98–0.99	21.95–23.36	29.97–30.07	30.60–30.86
RLG1 qAB140/141	95.17–97.87	−3.69 to −3.60	25.01–25.76	0.98–0.99	23.46–26.71	32.28–32.92	33.64–35.96
SCR1 qAB98/99	94.30–96.65	−3.68 to −3.76	15.24–15.81	0.98–0.99	13.26–15.10	31.42–32.29	32.66–34.68
KAR2 qAB104/105	83.42–96.94	−3.86 to −3.39	16.33–17.85	0.98–0.99	14.70–18.15	30.53–31.37	35.51–35.13
PDI1 qAB 108/109	91.22–102.61	−3.55 to −3.23	17.42–19.48	0.98–0.99	19.21–21.41	33.25–33.55	35.98–37.44
18S qAB8/9	97.18–103.97	−3.23 to −3.161	9.24–10.98	0.98–0.99	9.82–12.006	31.25–32.21	32.22–33.22
RRP6 qAB116/117	95.88–97.66	−3.42 to −3.37	21.95–22.11	0.98–0.99	20.89–23.72	32.36–32.41	32.54–32.65
SNR37 qAB246/247	99.65–102.25	−3.45 to −3.431	28.21–28.99	0.98–0.99	21.15–23.54	36.54–37.69	37.87–38.10
SNR37ETS qAB248/249	94.25–98.25	−3.08 to −3.06	40.25–40.2	0.98–0.99	25.31–34.60	36.33–37.20	37.35–37.40
3′UTR *HAC1* AB357/350	97.70–98.37	−3.47 to −3.43	32.38–33.24	0.95–0.97	25.10–26.72	31.34–31.85	31.44–31.54

carried out using divalent cations under elevated temperature in NEBNext First Strand Synthesis Reaction Buffer (5×). First strand cDNA was synthesized using random hexamer primer and M-MuLV Reverse Transcriptase (RNase H-). Second strand cDNA synthesis was subsequently performed using DNA Polymerase I and RNase H. Remaining overhangs were converted into blunt ends via exonuclease/polymerase activities. After adenylation of 3′ ends of DNA fragments, NEBNext Adaptor with hairpin loop structure were ligated to prepare for hybridization. In order to select cDNA fragments of preferentially 150∼200 bp in length, the library fragments were purified with AMPure XP system (Beckman Coulter, Beverly, USA). Then 3 μl USER Enzyme (NEB, USA) was used with size-selected, adaptor ligated cDNA at 37°C for 15 min followed by 5 min at 95°C before PCR. Then PCR was performed with Phusion High-Fidelity DNA polymerase, Universal PCR primers and Index (X) Primer. At last, PCR products were purified (AMPure XP system) and library quality was assessed on the Agilent Bioanalyzer 2100 system. A 150 bp read sequencing was Illumina sequenced with multiplexing. A mean of 17.7 ± 2.4 million passing Illumina quality filter reads was obtained for each of the samples.The clus-

Table 5. Antibodies used in this study

Antibody	Reference	Dilution
Peroxidase AffiniPure Goat Anti-Mouse IgG (H + L)	Jackson ImmunoResearch – 115-035-003	1:10 000
Peroxidase AffiniPure Goat Anti-Rabbit IgG (H + L)	Jackson ImmunoResearch – 115-035-144	1:10 000
Peroxidase AffiniPure Goat Anti-Rat IgG (H + L)	Jackson ImmunoResearch – 115-035-143	1:10 000
Anti-Pdi1	Invitrogen – MAI-10 032	1:2000
Anti-Pab1	Abcam – ab 189 635	1:10 000
Anti-Tub1	Santa Cruz – sc 53 030	1:2000
Anti-Hac1	Peter Walter (5)	1:8000
Anti-Rrp6	T.H Jensen	1:2000

tering of the index-coded samples was performed on a cBot Cluster Generation System using PE Cluster Kit cBot-HS (Illumina) according to the manufacturer's instructions. After cluster generation, the library preparations were sequenced on an Illumina platform and paired-end reads were generated.

Next-generation sequence analysis

For RNA-seq analysis, raw data were processed through in-house scripts. Paired-end clean reads were mapped to the reference genome using HISAT2 software. Reads were aligned to the *S. cerevisiae* reference genome (SaCer3). HTSeq software was used to analyze the gene expression levels in this experiment, using the union mode. Differential expression analysis between two conditions (three biological replicates per condition) was performed using DESeq2, R package. The resulting *P*-values were adjusted using the Benjamini and Hochberg's approach for controlling the false discovery rate. Genes with an adjusted *P*-value < .05 found by DESeq2 were assigned as differentially expressed.

Protein analyses

Cells grown to OD_{600} = 0.4 were treated or not with ER stress-inducing agents for the indicated time. For each time point, 10 OD of cells were collected and precipitated with 20% trichloroacetic acid (TCA; Sigma). Cells were pelleted and washed in 20% TCA at 4°C, and snap frozen in liquid nitrogen. After resuspension in 200 µl of TCA 20% cells disruption was performed by bead beating at 4°C in the presence of 100 µl of acid washed glass beads (Sigma). After beads removal, samples were clarified by centrifugation at 11 000 × *g* for 10 min and pellets were resuspended in Laemmli buffer, heated for 5 min at 95°C. Protein samples were separated by sodium dodecyl sulphate–polyacrylamide gel electrophoresis and transferred onto a nitrocellulose membrane that was probed with the relevant antibody. Proteins were detected by chemiluminescence (SuperSignal™ West Pico/Femto Chemiluminescent Substrate, Thermo Fisher) and images were captured with the FUSION FX imaging system (Vilber) or a ChemiDoc MP Imaging System (Bio-Rad). Antibodies used in this study are described in Table 5.

Statistics and reproducibility

Every depicted blot represents one of at least three independent experiments. Plots and statistical analysis were performed using Excel (Microsoft) for qRT-PCR analysis or Prism (Graphpad) for RNA-seq analysis. Statistic tests and *P*-values are described in the figure legends. Significance of the observed differences (**P*-value = .01–.05; ***P*-value = .001–.01; ****P*-value < .001). For each experiment, the value of every data point as well as *P*-values are provided in the source data file and the figure legend.

Results

Cells inactivated for the exonuclease activities of the RNA exosome show increased resistance to ER stress

To investigate how Rrp6 influences the UPR, we first analyzed the physiological consequences of *RRP6* inactivation. Under basal conditions, *rrp6*Δ cells presented a growth defect that was rescued upon expression of wild-type *RRP6* but not the catalytically inactive allele *rrp6D238A* as previously reported [35, 36]. Examination of cells' growth and viability in the presence of Tm, a well-established inhibitor of N-linked glycosylation that induces the accumulation of unfolded proteins in the ER, confirmed that cells inactivated for *RRP6* display better growth (Fig. 1A) and viability (Fig. 1B) than wild-type (WT) cells and revealed that this resistance depends on Rrp6 catalytic activity [35] (Fig. 1A). Resistance to Tm was also observed when Rrp6 was depleted through an Rrp6 auxin degron [33] (Fig. 1C and Supplementary Fig. S1A and B) or when its ribonucleolytic activity was inhibited by growth in the presence of the pyrimidine analog 5-fluorouracil (5FU) [37, 38] (Fig. 1D and Supplementary Fig. S1C). In cells inactivated for *LRP1/RRP47*, which encodes a Rrp6 co-factor whose direct interaction with Rrp6 stabilizes it [39, 40] or for *TRF4*, a polyA-polymerase component of the TRAMP complex that stimulates the exonuclease activity of the RNA exosome [41, 42], resistance to Tm was also observed, although to a lesser extent than for *rrp6*Δ cells (Fig. 1E). Noteworthy, in these cells, the steady-state level of Rrp6 was decreased compared to that of WT cells (Supplementary Fig. S1D). These results collectively suggest that the Tm resistance phenotype observed upon *RRP6* inactivation does not result from a secondary mutation but from the absence of its catalytic activity. We next addressed whether the inactivation of Dis3, the other catalytic subunit of the RNA exosome that displays both endo and exonuclease activities (see positions of the catalytic sites' mutations on Fig. 1F, upper panel), similarly conferred resistance to ER stress. Because the combined inactivation of both Dis3 catalytic domains is lethal [43], we first compared the Tm sensitivity of strains constitutively expressing either the D171N mutation in the endonucleolytic domain (endo-) or the wild-type allele (*DIS3*) [44] (Fig. 1F, middle panel). We then used strains expressing the D551 mutation in the exonucleolytic domain (*dis3 exo-*), the D551 and D171N mutations (*dis3 endo-exo-*) or wild-type *DIS3*, in a background allowing the repression of wild-type *DIS3* through a doxycycline repressible promoter (Fig. 1F lower panel, S1E) [43]. While *dis3 endo-* cells showed similar Tm sensitivity to wild-type, *dis3 exo-* cells were more resistant, albeit to a lesser extent than *rrp6*Δ cells. This difference in ER stress resistance observed among RNA exosome mutants is consistent with the fact that the two catalytic subunits of the complex have both overlapping and specific roles in degrading distinct classes of substrates [29]. Cells inactivated for both the endo and exonucleolytic domains presented a growth defect that was independent of the presence of Tm in the growth medium.

Finally, to probe for the specificity of this phenotype, we analyzed the Tm sensitivity of a sample of RNA metabolism mu-

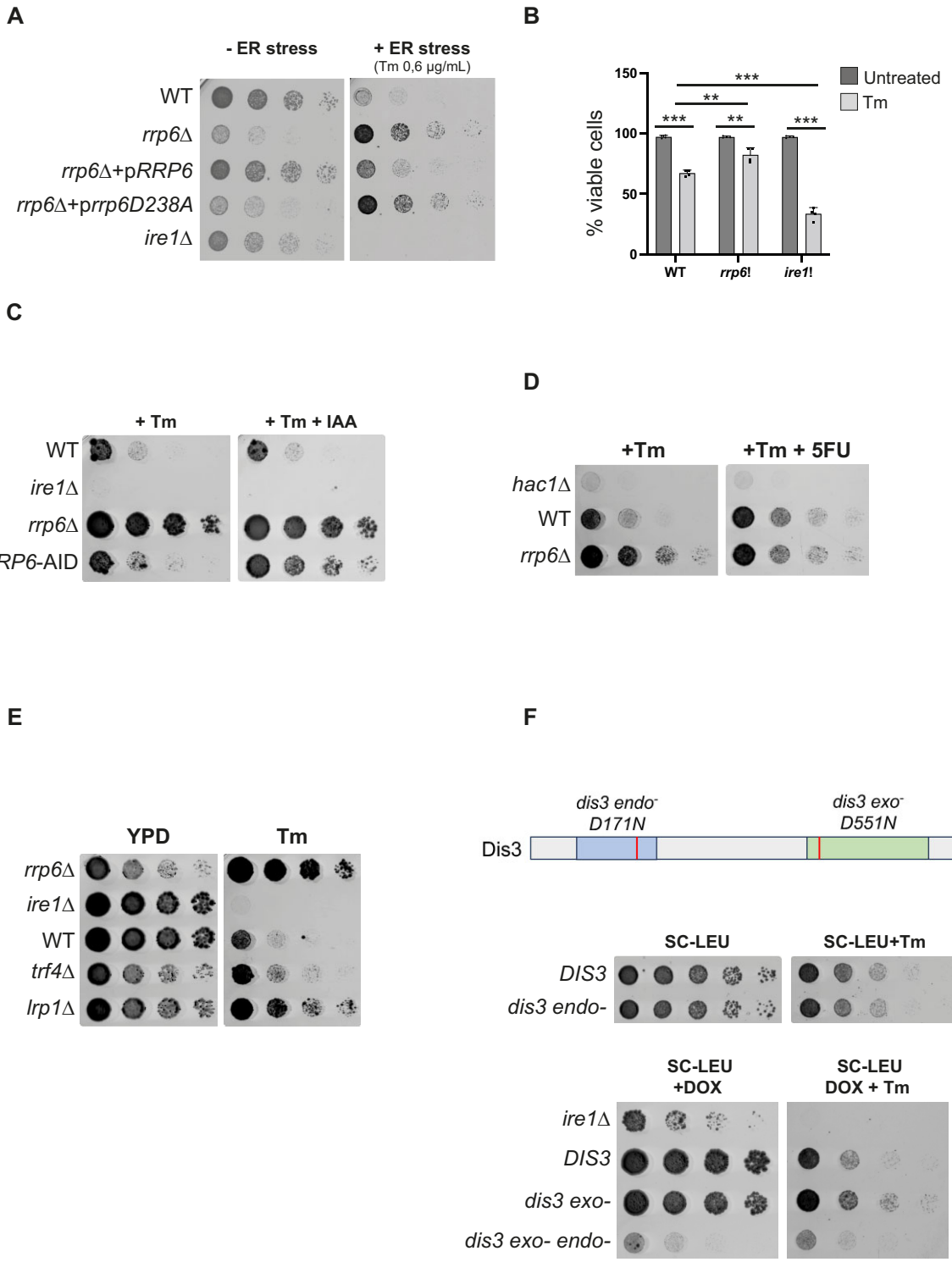

Figure 1. Cells inactivated for the exonuclease activities of the RNA exosome show increased resistance to ER stress. (**A**) ER stress sensitivity assay: five-fold serial dilutions of the indicated strains grown for 3 days at 30°C on selective media containing (+ER stress) or not (−ER stress) 0.6 µg/ml Tm. (**B**) Viability assay. Exponentially growing cells were treated or not with 1 µg/ml Tm for 24 H and stained with PI. The percentage of PI negative cells is plotted. A minimum of 300 cells per condition were counted. $n = 4$ independent experiments, mean ± standard deviation (SD). Unpaired one-tail *t*-test. (*P*-values for Tm relative to Untreated: 3.01E-07, 1.23E-03, and 1.49E-07 for WT, *rrp6*Δ, and *ire1*Δ respectively. *P*-values for mutants relative to WT upon Tm treatment: 1.68E-03 and 8.15E-06 for *rrp6*Δ, and *ire1*Δ). (**C**) Five-fold serial dilutions of the indicated strains grown for 3 days at 30°C on YPD media containing 0.6 µg/ml Tm or 0.6 µg/ml Tm plus 500 µM indole-3-acetic acid (IAA). (**D**) Five-fold serial dilutions of the indicated strains grown for 3 days at 30°C on YPD media containing 0.6 µg/ml Tm or 0.6 µg/ml Tm plus 6 µM 5FU. Note that 5FU does not affect the growth of these strains on YPD (Supplementary Fig. S1C) nor that of *rrp6*Δ cells on YPD +Tm as expected. (**E**) Five-fold serial dilutions of the indicated strains grown for 3 days at 30°C on YPD media containing or not 0.6 µg/ml Tm. (**F**) Up: Scheme showing the positions of the mutations inactivating the endonucleolytic and exonucleolytic activities of Dis3. Middle: Five-fold serial dilutions of the indicated strains grown for 3 days at 30°C on SC-LEU media with or without 0.6 µg/ml Tm. Down: Five-fold serial dilutions of the indicated strains grown for 3 days at 30°C on SC-LEU media containing 10 µg/ml doxycycline with or without 0.6 µg/ml Tm.

tants previously reported as 'resistant' in genome-wide analysis [30]. We observed resistance to Tm neither for cells deprived of the tRNA:pseudouridine synthase Deg1 [45], nor of the tRNA exportin Los1 [46], nor of the nonsense-mediated mRNA decay factor Nmd2 [47], nor the 5′-3′ exonuclease Xrn1 [48] (Supplementary Fig. S1F). Because they target distinct RNA substrates, these different enzymes are unlikely to impact the *HAC1* splicing machinery similarly. Collectively, these results suggest that resistance to ER stress does not result from global RNA metabolism alterations but is rather specific to compromised exonucleolytic activity of the RNA exosome.

The ER stress resistance of cells lacking *RRP6* is UPR dependent and does not result from an increased pool of spliceable *HAC1* transcripts

Although consistent with previous reports [30, 31], the phenotype of *rrp6Δ* cells was intriguing because it is opposite to that observed for *isw1Δ* cells [12]. Given the central role of Rrp6 in pre-rRNA processing [49, 50] and the reported protective effect of cycloheximide-induced inhibition of protein synthesis or ribosome deficiency toward ER stress [51], we asked whether the resistance of *rrp6Δ* cells could result from defective ribosomal RNA maturation, independently of the UPR. Contrary to cells inactivated for ribosomal protein genes, which show resistance to ER stress even upon UPR inactivation [51], we observed that *IRE1* inactivation sensitized *rrp6Δ* cells to ER stress (Fig. 2A), indicating that their ER stress resistance is UPR dependent, and suggesting that it does not simply result from defective rRNA biogenesis.

The resistance of *rrp6Δ* cells to ER stress was proposed to arise from *HAC1* mRNA stabilization, resulting in an increase in the pool of full-length transcripts harboring a 3′BE sequence and thus competent for Ire1-mediated splicing [31] (Fig. 2B). Using phenanthroline to inhibit transcription, we compared the stability of the unspliced (*HAC1*u for **u**nspliced) and spliced (*HAC1*s for **s**pliced) forms of the *HAC1* transcript by monitoring their expression level by RT-qPCR using previously described specific primers [12] (Fig. 2C). In the absence of ER stress, we observed a stabilization of *HAC1u* in *rrp6Δ* cells compared to WT, as previously described [31]. However, DTT—a reducing agent and potent ER stress-inducer that blocks disulfide bonds' formation—stabilized *HAC1*u such that its stability was indistinguishable between WT and *rrp6Δ* cells. Similarly, no difference in the stability of *HAC1*s was detected in the presence of DTT between WT and *rrp6Δ* cells (Fig. 2D and Supplementary Fig. S2A). We also examined the stability of *PMA1* and *CYC1*, two UPR-unrelated transcripts previously reported as Rrp6-sensitive and insensitive, respectively [52]. *PMA1*, like *HAC1*, was stabilized upon *RRP6* inactivation and ER stress, while their effects on *CYC1* stability were modest. In addition, *CYC1* transcript presented similar decay rates under control and ER stress conditions, indicating that phenantroline treatment equally affected transcription under these different experimental settings (Supplementary Fig. S2B). Finally, we sought to identify an increased pool of full-length 3′BE-containing *HAC1* transcript in *rrp6Δ* compared to WT cells using RT-qPCR (see Fig. 2E lower panel for primers positions). However, no difference in the abundance of the 3′BE-containing 3′UTR relative to the 5′ end of the *HAC1* transcript could be detected under basal conditions by RT-qPCR in WT or *rrp6Δ* cells. In contrast, in the same samples, the accumulation of previously reported extended snR37 transcripts [53] was readily detected in *rrp6Δ* cells compared to WT (Fig. 2E).

Together, while confirming that in the absence of ER stress, *HAC1* mRNA stability is influenced by Rrp6, these results indicate that *RRP6* inactivation increases cells' resistance to ER stress in a UPR-dependent manner and that stabilization of the *HAC1* transcript may not be solely responsible for this resistance.

RRP6 inactivation fosters restoration of ER homeostasis and UPR termination

Having previously reported that the kinetics of ER homeostasis recovery was delayed in cells with increased sensitivity to ER stress, we next asked whether conversely, cells with increased resistance to ER stress would show faster ER homeostasis recovery. To this aim, we used an established assay monitoring the glycosylation state of protein disulfide isomerase 1 (Pdi1) as a read-out for the ER folding status during a UPR time-course [12]. In this previously set up UPR time-course, ER stress was induced by a 2-hour Tm treatment that does not affect cell viability (Supplementary Fig. S3A), followed by a wash of the drug from the medium, thereby allowing analysis of the activation and termination phases of the UPR (Fig. 3A). Pdi1 is an ER luminal molecular chaperone that catalyzes disulfide bonds' formation and contains five acceptor sites for N-glycans. As previously observed [12], Tm treatment inhibited Pdi1 glycosylation, detected after 2H as two bands corresponding to the fully glycosylated and unglycosylated forms of the protein in both WT and *rrp6Δ* cells. Upon removal of the drug, Pdi1 progressively recovered its initial glycosylation status in both cell types. Strikingly, the recovery was faster in *rrp6Δ* cells than in WT (Fig. 3B and C), suggesting that in these cells, the re-establishment of the oxidative protein folding capacity of the ER was accelerated compared to WT cells, in line with their enhanced resistance to Tm.

To elucidate the grounds for the resistance of *rrp6Δ* cells to ER stress, we set out to analyze their transcriptional UPR output, using the above described Tm time-course that allows to observe complete UPR activation and deactivation within 6H by RT-qPCR [12] (Fig. 3A). In WT cells, as expected, Tm induced the production of the spliced form of *HAC1, HAC1s,* which reached a maximum after 2H and was followed by a gradual decline upon wash of the drug (Supplementary Fig. S3B). In the absence of ER stress, the basal level of *HAC1*s was increased in *rrp6Δ* cells compared to WT, which likely results from the stabilization of the transcript and its subsequent splicing by Ire1 basal activity [54] (Supplementary Fig. S3B). In contrast, during the adaptation phase of the UPR, the level of *HAC1*s was significantly reduced in *rrp6Δ* compared to WT cells (Supplementary Fig. S3B). In addition, the fold induction of *HAC1*s was significantly lower in *rrp6Δ* cells than in WT cells (Fig. 3D). As such, the percentage of spliced *HAC1* (% *HAC1*s) was significantly decreased in *rrp6Δ* cells compared to WT (Fig. 3E) and, accordingly, the expression of the Hac1 protein (Fig. 3F) and of *KAR2* and *PDI1,* two *bona fide* Hac1 transcriptional targets (Fig. 3G), decreased faster in *rrp6Δ* compared to WT cells in the course of the experiment. It is worth noting that the increased basal *HAC1*s level observed in *rrp6Δ* cells was insufficient to allow for the detection of the Hac1 protein in the absence of stress (Fig. 3F lane 2). To further corroborate these results, genome-wide expres-

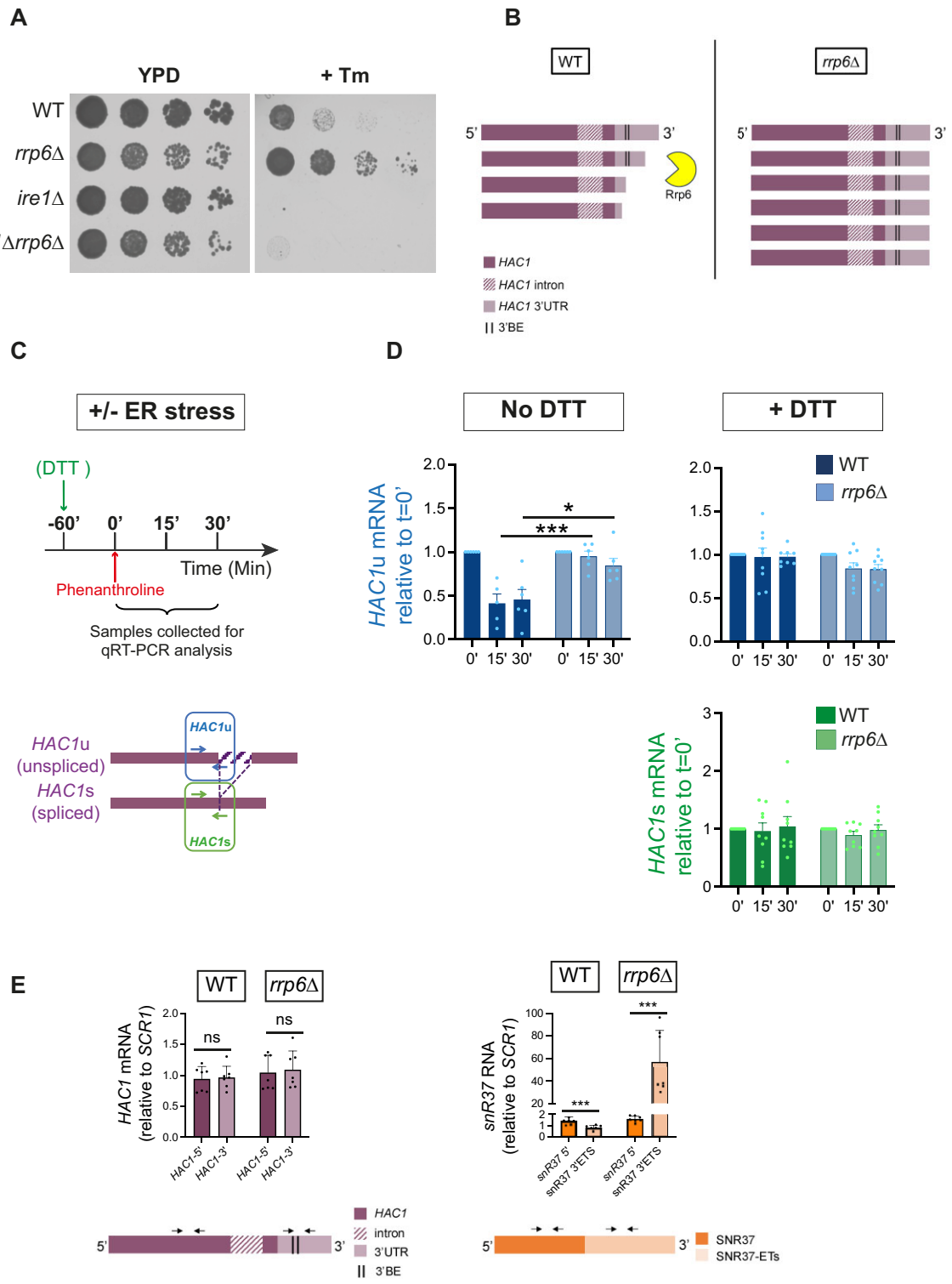

Figure 2. The ER stress resistance of cells lacking *RRP6* is UPR dependent and does not result from an increased pool of spliceable *HAC1* transcripts. (**A**) The Tm resistant phenotype of *rrp6*Δ cells is Ire1 dependent: five-fold serial dilutions of the indicated strains grown for 3 days at 30°C on YPD media containing or not 0.6 μg/ml Tm. (**B**) Schematic illustration of a proposed model [31] according to which the exonuclease activity of Rrp6 generates a pool of nonspliceable *HAC1* transcipts devoid of the 3′BE element, that allows targeting to Ire1 for optimal splicing. (**C**) Scheme depicting the principle of transcripts stability analysis: *rrp6*Δ and WT cells were treated (+ER stress) or not (−ER stress) with DTT for 1H and transcription was inhibited by addition of 0.2 mg/ml phenanthroline (t = 0). Samples were collected for analysis at t = 0′, 15′, and 30′. RT-qPCR analyses were performed using primers specific for the unspliced (*HAC1*u, blue) and spliced (*HAC1*s, green) forms of *HAC1* mRNA. (**D**) RT-qPCR analysis of *HAC1*s and *HAC1*u mRNA levels in WT and *rrp6*Δ cells, in *n* = 6–9 independent experiments, mean ± SD. Unpaired one-tailed *t*-tests (No ER stress *HAC1*u *P*-values *rrp6*Δ relative to WT: 5.81E-04, 1.04E-02; ER stress *HAC1*u *P*-values *rrp6*Δ relative to WT: 1.5.E-01, 6.1.E-02; ER stress *HAC1*s *P*-values *rrp6*Δ relative to WT: 3.27.E-01, 3.77.E-01). Unnormalized values are presented in Supplementary Fig. S2A. (**E**) RT-qPCR analysis of the expression of 3′ versus 5′ ends of *HAC1* and *snR37* transcripts in *n* = 7 independent experiments, mean ± SD. Unpaired one-tailed *t*-tests (WT *P*-values 3′ relative to 5′: 4,10E-01 and 6,70E-04 for *HAC1* and *snR37* respectively; *rrp6*Δ *P*-values 3′ relative to 5′: 3,87E-01 and 1,04E-04 for *HAC1* and *snR37*).

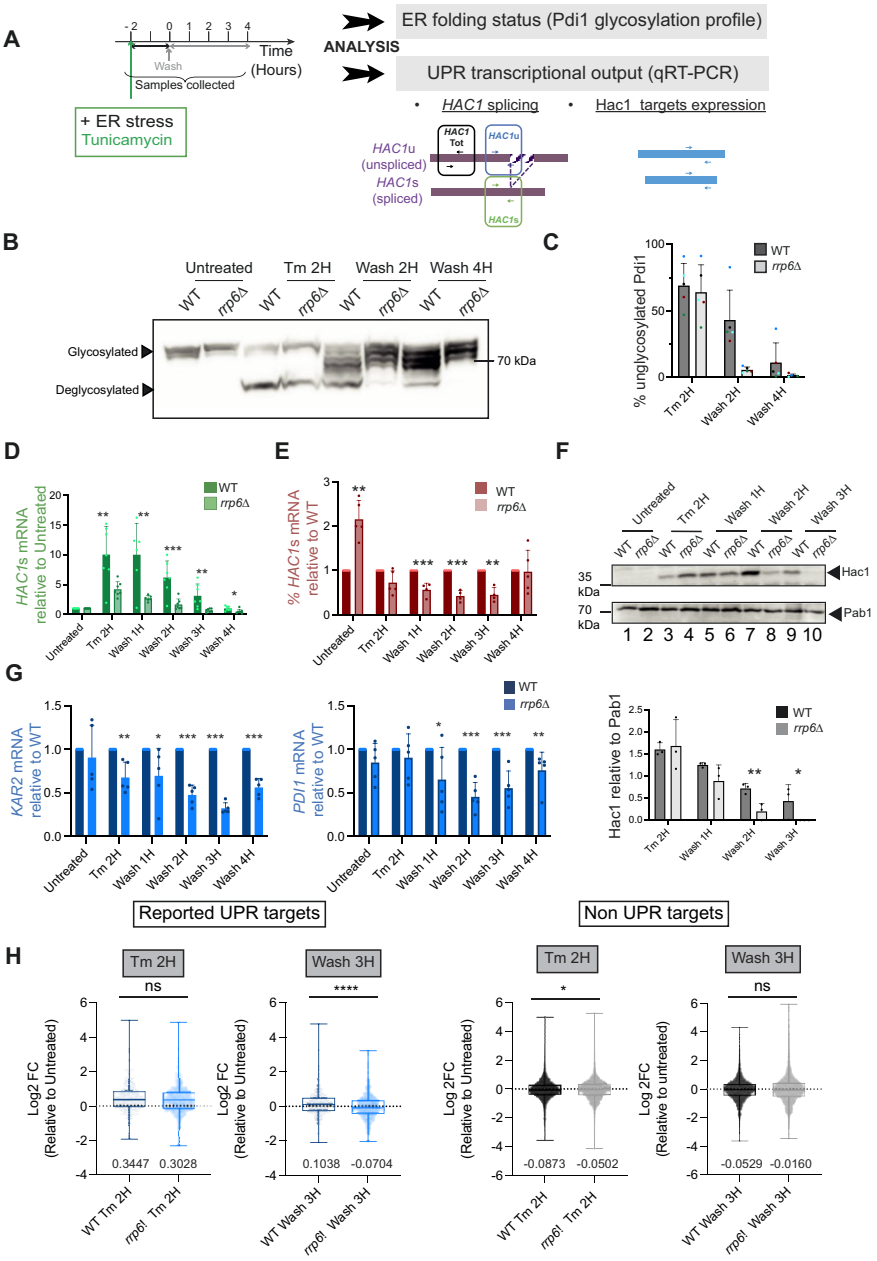

Figure 3. *RRP6* inactivation fosters restoration of ER homeostasis and UPR attenuation. (**A**) Tm UPR time course experimental setting: exponentially growing cells were treated with 1 μg/ml Tm for 2H, washed, and resuspended in Tm free medium. Samples were collected at t = −2H (Untreated), t = 0 (Tm 2H), t = 1H (Wash 1H), t = 2H (Wash 2H), t = 3H (Wash 3H), and t = 4H (Wash 4H) for analysis of Pdi1 glycosylation status by western blot or for analysis of *HAC1* mRNA splicing and expression of UPR target genes by RT-qPCR using the depicted primers. (**B**) Pdi1 reglycosylation during Tm UPR time course. Total protein extracts from WT and *rrp6*Δ cells collected during Tm UPR time courses were analyzed by western blot with anti-Pdi1 antibodies. (**C**) The level of fully deglycosylated Pdi1 was quantified across five independent Tm UPR time course. $n = 5$, mean ± SD. Unpaired one-tail *t*-test (*P*-values relative to WT: 3.42E-01, 2.94E-03, and 2.93E-02 for Tm 2H, Wash 2H, Wash 4H, respectively). (**D**) Fold induction of *HAC1*s in *rrp6*Δ and WT cells. $n = 7$ independent experiments, mean ± SD. Unpaired one-tail *t*-test (*P*-values relative to WT: 4.19E-03, 4.29E-03, 7.62E-04, 3.61E-03 and 1,20E-02 for Tm 2H, Wash 1H, Wash 2H, Wash 3H, Wash 4H, respectively). Unnormalized values are presented in Supplementary Fig. S3B. (**E**) The percentage of spliced *HAC1* was calculated from the values obtained in Supplementary Fig. S3B. $n = 5$ independent experiments, mean ± SD. Unpaired one-tail *t*-test (*P*-values relative to WT: 4.16E-01, 8.09E-02, 6.83E-03, and 5.60E-02 for Untreated, Tm 2H, Wash 1H, Wash 2H, Wash 3H, Wash 4H, respectively). (**F**) Total protein extracts from WT and *rrp6*Δ cells treated or not with 1 μg/ml Tm for 2 H were analyzed by western blot with anti-Hac1 and Pab1 (loading) antibodies. The level of Hac1 and Pab1 was quantified. $n = 4$ independent experiments, mean ± SD. Unpaired one-tail *t*-test (*P*-values relative to WT: 3.33E-01, 1.92E-03, 3.39E-02, 3.68E-04 at Tm 2H, Wash 2H, Wash 3H, respectively). (**G**) RT-qPCR analysis of the expression levels of *KAR2* and *PDI1* normalized by *SCR1* relative to WT, in WT and *rrp6*Δ cells during the Tm UPR time course depicted in panel (A). $n = 5$ independent experiments, mean ± SD. Unpaired one-tail *t*-test (*P*-values relative to WT: 2.95E-01, 1.70E-03, 3.22E-02, 3.37E-06, 5.25E-09, and 5.73E-06 for *KAR2* and 6.14E-02, 2.07E-01, 2.28E-02, 9.04E-06, 1.66E-04, and 9.57E-03 for *PDI1*). (**I**) Whisker plots of expression fold change (log_2 FC) for all UPR (defined in [7]) and non-UPR target genes at Tm 2H and Wash 3H relative to untreated in WT and *rrp6*Δ cells. Boxes extend from the 25th to 75th percentiles. The line in the middle of the box is plotted at the median. Median values are provided below each box. Whiskers are plotted down to the minimum and up to the maximum value, and each individual value is plotted as a point superimposed on the graph. $n = 3$ independent biological replicates. Unpaired two-tailed Mann–Whitney test (*P*-values for UPR targets: 0.38 and < 1.00E-04 for Tm 2H and Wash 3H, respectively; *P*-values for non-UPR targets: 0.0201 and 0.9346 for Tm 2H and Wash 3H, respectively).

sion profiling of WT and *rrp6Δ* cells was performed across similar (Untreated, Tm 2H, Wash 3H) UPR time courses (Fig. 3H). This revealed that the expression fold-change of UPR target genes relative to untreated conditions was similar in WT and *rrp6Δ* cells after a 2-hour Tm treatment, confirming that UPR is similarly induced in both cell types. Strikingly, during the deactivation phase of the UPR (Wash 3H), the expression fold-change of UPR target genes relative to untreated conditions was significantly lower in *rrp6Δ* compared to WT cells, indicating that *RRP6* inactivation coincides with faster UPR deactivation. Of note, no significant difference was observed in the expression fold-change of non-UPR target genes relative to untreated conditions, neither after a 2-hour Tm treatment nor 3H after wash and removal of Tm from the medium, between WT and *rrp6Δ* cells. Hence, this underlies the specificity of *RRP6* inactivation on the kinetics of UPR genes' expression attenuation. Finally, triggering the UPR with DTT recapitulated the effect of Tm (Supplementary Fig. S3D–G), indicating that the phenotype of *rrp6Δ* cells is not specific to Tm but rather to ER stress. Thus, *RRP6*-inactivated cells activate the UPR to a similar extent as WT cells but terminate it faster and are more resistant to ER stress.

Shorter UPR signaling rather than hormesis allows *rrp6*Δ cells resistance to ER stress

Conditions that induce mild ER stress can engage adaptative signaling events, thereby conferring cells' resistance to higher doses of ER stress, a phenomenon referred to as ER hormesis [55–57]. The higher basal expression of *HAC1*s observed in cells inactivated for *RRP6* compared to WT (Supplementary Fig. S3B right, compare *HAC1s* mRNA Untreated for WT and *rrp6*Δ) suggested that *RRP6* inactivation may confer protection against ER stress through hormesis. To address this possibility, we sought to analyze the resistance to ER stress of *rrp6Δ* cells displaying the same basal level of spliced *HAC1* as WT cells. Guided by our transcriptional analysis that indicated a similar level of *HAC1*s between both strains after a 2-hour Tm induction followed by a wash of the drug and subsequent growth in a Tm-free medium for 4H (Supplementary Fig. S3B right, compare *HAC1s* mRNA Wash 4H for WT and *rrp6*Δ), we preconditioned WT or *rrp6Δ* cells using this protocol (Fig. 4A) and subsequently analyzed their sensitivity to Tm. Under this regimen, *rrp6Δ* cells still showed increased resistance to ER stress compared to WT (Fig. 4B), indicating that basal UPR induction is not the main driver of *rrp6Δ* cells' resistance to ER stress. Interestingly, the absence of a direct causal relationship between basal UPR activity and resistance to ER stress is also supported by our former results showing that despite increased basal *HAC1*s expression, *isw1Δ* cells display increased ER stress sensitivity [12].

We next asked whether the Tm resistance phenotype of *rrp6Δ* cells could alternatively result from their faster UPR deactivation. To this aim, we created an Ire1 version that contained an auxin-inducible degron (AID) module that can be depleted on-demand by auxin addition. The AID tag was inserted into the cytosolic portion of Ire1 adjacent to its transmembrane region to preserve the protein function (Supplementary Fig. S4A). Cells expressing this AID-tagged version of Ire1 showed WT resistance to ER stress (Supplementary Fig. S4B), indicating an unaltered ability to activate UPR. When the Tir1 F-box protein from *Oryza sativa* (OsTir1) was expressed in these cells, Ire1-AID was rapidly depleted upon auxin addition (Fig. 4C). As expected, when plated onto Tm-containing plates in the presence of IAA (auxin), they showed marked sensitivity to Tm, comparable to that of *ire1Δ* cells (Fig. 4D, +Tm +IAA). Using this system to force UPR termination artificially, we analyzed cell viability after 24H Tm treatment upon continuous UPR signaling or when UPR was interrupted 2H after Tm addition (Fig. 4E) via auxin-mediated Ire1 degradation. Strikingly, the viability of cells for which UPR was prematurely interrupted by auxin addition (Fig. 4F, left panel)—and therefore following Ire1 degradation (Supplementary Fig. S4C)—was significantly increased compared to those with natural UPR termination. Importantly, auxin did neither affect the viability of unstressed *IRE1-AID* cells nor that of stressed or unstressed *ire1Δ* cells (Fig. 4F, right panel).

Altogether, these data indicate that premature UPR termination benefits cell survival upon ER stress and suggest that premature UPR termination in *rrp6Δ* cells significantly contributes to their increased resistance to ER stress.

Reduced *HAC1* splicing in *rrp6*Δ cells stems from an out titration of its splicing machinery

Next, we investigated the molecular mechanisms underlying the reduced splicing of *HAC1* mRNA observed in *rrp6Δ* cells compared to WT during Tm-induced UPR time courses (Fig. 3D). We reasoned that it could, in principle, result from either a reduced expression of *HAC1* mRNA splicing machinery (Ire1, Trl1/Rlg1) or from a decrease in its activity. However, RT-qPCR analysis of *TRL1/RLG1* and *IRE1* expression levels in the same Tm time courses that unveiled a significantly decreased expression of UPR target genes revealed no significant differences between WT and *rrp6Δ* cells (Fig. 5A), suggesting that the decreased *HAC1* mRNA splicing observed in *rrp6Δ* cells is likely driven by defective splicing activity. Given that reduced accumulation of *HAC1*s mRNA cannot directly reflect the loss of Rrp6 activity and in light of recent studies demonstrating how the unscheduled persistence of unprocessed RNAs caused by *RRP6* inactivation can sidetrack cellular RNA-binding proteins from their normal function [58–61], we hypothesized that such RNA species could similarly divert the *HAC1* mRNA splicing machinery.

First, since tRNAs are processed by Rrp6 and given that both tRNAs and *HAC1* mRNA are Trl1/Rlg1 substrates, we considered the possibility that Trl1/Rlg1 activity was limiting. We reasoned that if Trl1/Rlg1 activity is limiting in *rrp6Δ* cells due to an excess of pre-tRNA, it should be possible to recapitulate the effect of *RRP6* inactivation by artificially increasing the level of intron-containing pre-tRNA. To this aim, we took advantage of cells expressing a mutant version of *SEN2*, which encodes a catalytic subunit of tRNA splicing endonuclease [46] and was reported to accumulate large amounts of cytoplasmic pre-tRNA [62, 63] at the restrictive temperature (37°C). Monitoring pre-tRNA accumulation in *sen2-42* cells by RT-qPCR using primers specific for the unspliced forms of the tRNA LEU(CAA) not only confirmed this phenotype at restrictive temperature (Supplementary Fig. S5A) but also unexpectedly revealed significant accumulation of pre-tRNA LEU at 23°C in *sen2-42* cells compared to WT (Fig. 5B). Strikingly, *sen2-42* cells presented a marked resistance to Tm at both 23°C (Fig. 5C) and 37°C (Supplementary Fig. S5B), which correlated with a reduction of *HAC1* mRNA splicing

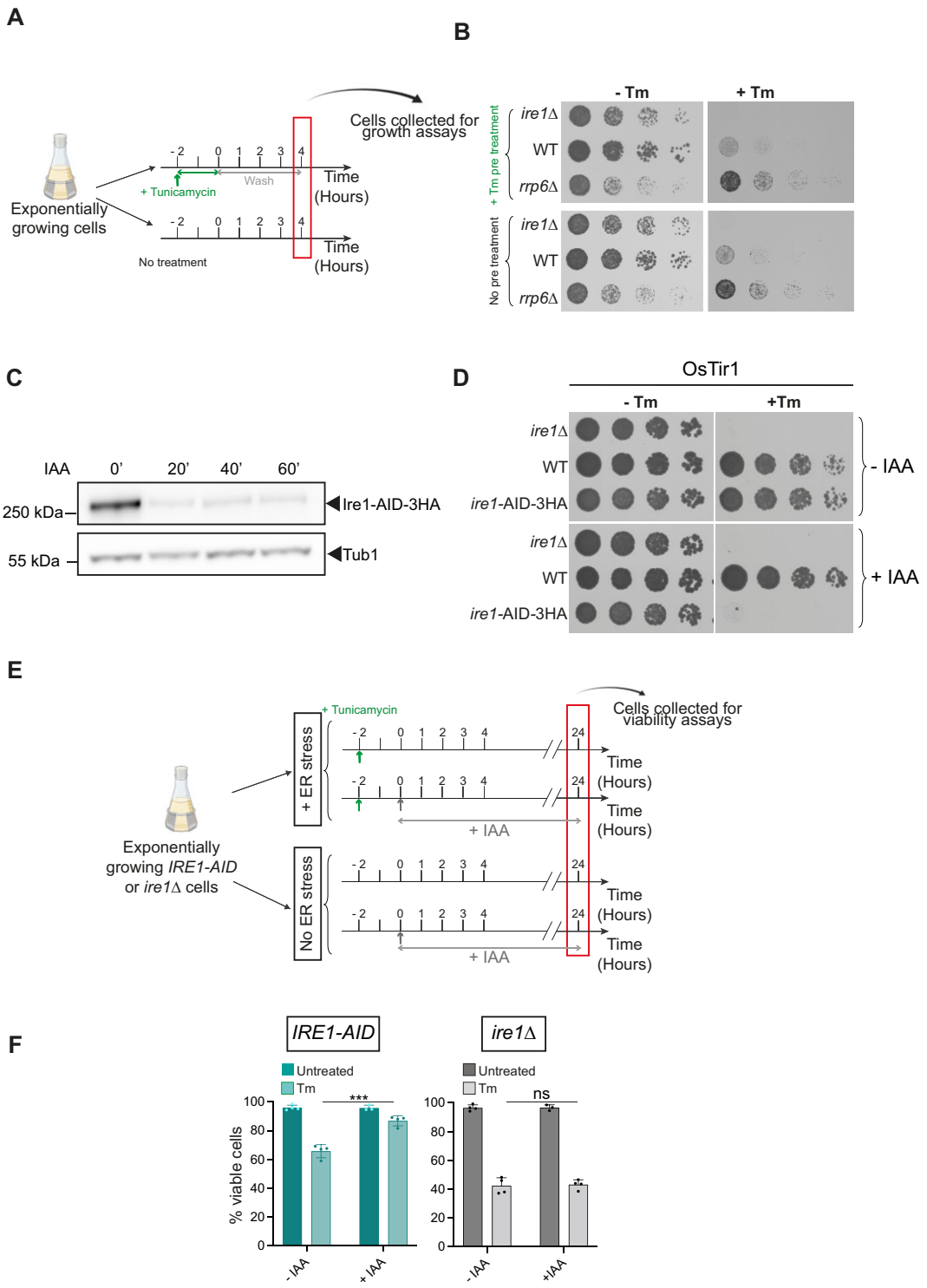

Figure 4. Limiting the duration of UPR signaling improves cells resistance to Tm. (**A**) Experimental setting: Exponentially growing cells are diluted to OD600 = 0.5, treated or not with 1 μg/ml Tm for 2H, washed and resuspended in Tm free media. After 4H, a time at which *rrp6*Δ cells express similar *HAC1*s level than WT cells (Fig. 3E), cells are collected and their sensitivity to Tm is analyzed. (**B**) The Tm resistance of *rrp6*Δ cells does not result from their increased basal expression of *HAC1*s compared to WT cells. Five-fold serial dilutions of the indicated strains grown for 3 days at 30°C on media containing (+ER stress) or not (−ER stress) 0.6 μg/ml Tm. (**C**) Total protein extracts from *IRE1*-AID cells expressing OsTir1 collected under untreated conditions and 20, 40, and 60 min after IAA treatment (500 μM) were analyzed by western blot with anti-HA (Ire1), and anti-Tub1 (loading) antibodies. (**D**) Five-fold serial dilutions of the indicated strains grown for 3 days at 30°C on YPD media containing (+ER stress) or not (−ER stress) 0.6 μg/ml Tm in the absence(−IAA) or presence of 500 μM IAA (+IAA). (**E**) Experimental setting: Exponentially growing cells are treated (+Tm) or not (−ER stress) with 1 μg/ml Tm. After 2H, 500 μM IAA were added to the cultures to trigger Ire1-AID degradation (+IAA) and thus interrupt UPR signaling or not (−IAA). Cells were collected at 24H for viability analysis. (**F**) Cells collected after the experimental treatment depicted in panel (E). were stained with PI. The percentage of viable cells (PI negative) is plotted. A minimum of 300 cells per condition were counted. $n = 4$ independent experiments, mean ± SD. Unpaired one-tail *t*-test (*P*-values +IAA relative to −IAA Ire1-AID: 4.61E-01, 1.64E-04 for Untreated and overnight Tm conditions, respectively; *P*-values +IAA relative to −IAA *ire1*Δ: 4.80E-01 and 4.08E-01 for Untreated and overnight Tm conditions, respectively).

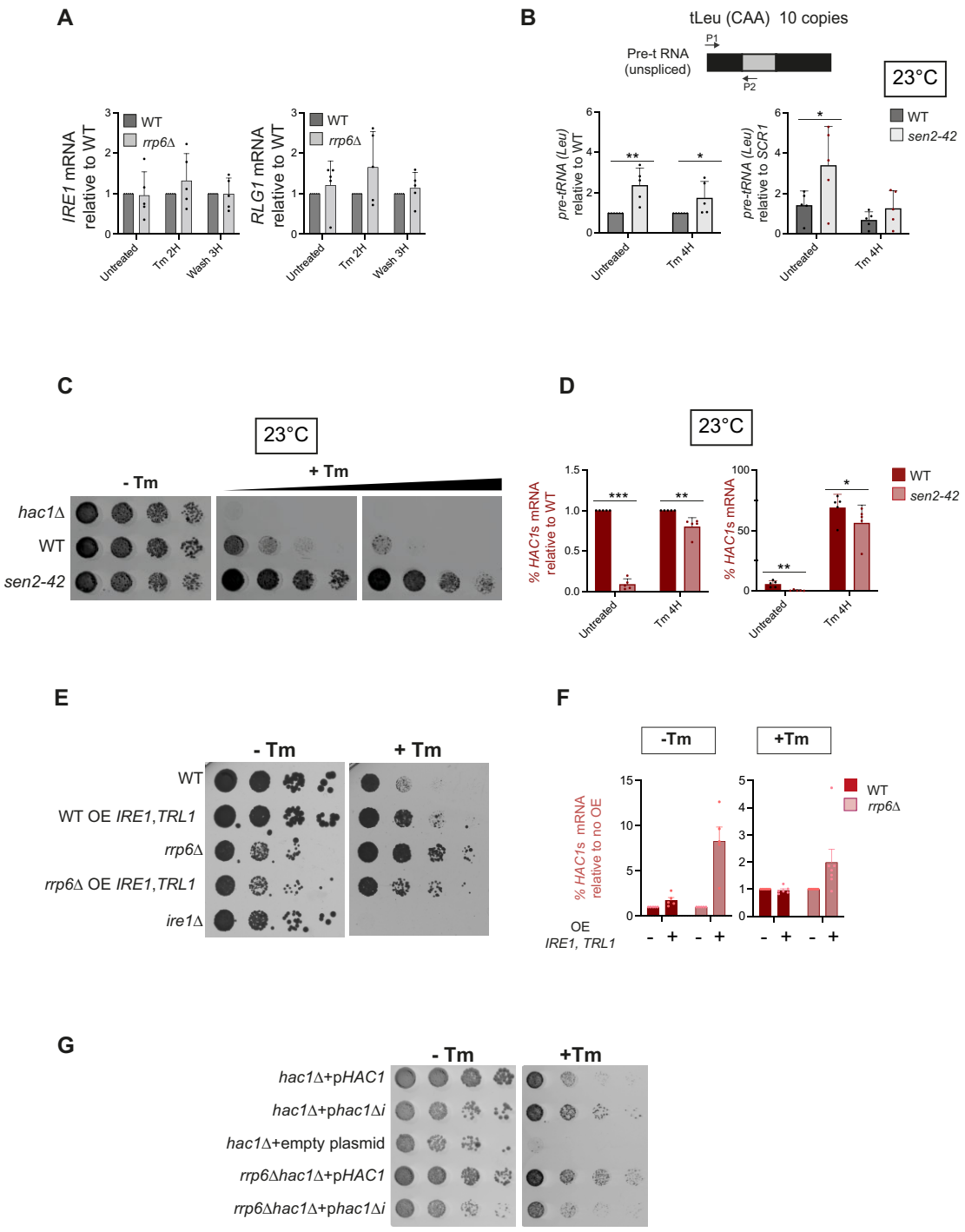

Figure 5. The ER stress resistance of *rrp6*Δ cells stems from an out titration of *HAC1* mRNA splicing machinery. (**A**) The expression level of *IRE1* and *RLG1* relative to 18S during Tm UPR time-course was measured by RT-qPCR in the indicated strains. $n = 5$ independent experiments, mean ± SD. Unpaired one-tailed *t*-tests (*P*-values for *IRE1*: 2.28E-01, 6.69E-02, 2.21E-01 for Untreated, Tm 2H, Wash 3H, respectively; *P*-values for *RLG1*: 4.38E-01, 1.55E-01, 4.89E-01 for Untreated, Tm 2H, Wash 3H, respectively). (**B**) RT-qPCR analysis of pre-tRNA LEU (CAA) in WT and *sen2-42* cells grown at 23°C using the depicted primers in untreated conditions or after a 4H Tm treatment. $n = 5$ independent experiments, mean ± SD. Unpaired one-tail *t*-test (*P*-values relative to WT: 3.12E-03 and 3.65E-02 in untreated and Tm 4H conditions, respectively when normalized to WT and 3.12E-02 and 1.09E-01 without normalization (relative to *SCR1*)). (**C**) Five-fold serial dilutions of the indicated strains grown for 3 days at 23°C on YPD media containing (+Tm) or not (−Tm) 0.6–0.8 μg/ml Tm. (**D**) *HAC1* mRNA splicing evaluated by RT-qPCR in WT and *sen2-42* cells grown at 23°C as in Fig. 3E. $n = 5$ independent experiments, mean ± SD. Unpaired one-tail *t*-test (*P*-values relative to WT: 6.62E-10 and 1.81E-03 in untreated and Tm 4H conditions, respectively when normalized to WT and 1.15E-03 and 8.02E-02 without normalization). (**E**) Overexpression (OE) of *IRE1* and *RLG1* sensitizes *rrp6*Δ cells to Tm. Five-fold serial dilutions of the indicated strains grown for 3 days at 30°C on media containing (+ER stress) or not (−ER stress) 0.6 μg/ml Tm. (**F**) *HAC1* mRNA splicing was analyzed as previously described in WT and *rrp6*Δ cells overexpressing (OE *IRE1*, *RLG1* +) or not (OE *IRE1*, *RLG1*) *IRE1* and *RLG1* upon untreated conditions or upon 4H 1 μg/ml Tm treatment (+ER stress). $n = 5$ independent experiments, mean ± SD. Unpaired one-tail *t*-test (*P*-values relative to No OE: 1.70E-02, 7.55E-04 for WT and *rrp6*Δ cells, respectively, in untreated conditions; 2.40E-01 and 2.84E-02 for WT and *rrp6*Δ cells, respectively, upon 4H Tm treatment). (**G**) Five-fold serial dilutions of the indicated strains grown for 3 days at 30°C on media containing (+Tm) or not (−Tm) 0.6 μg/ml Tm.

(Fig. 5D, 23°C, and Supplementary Fig. S5C, 37°C) at both temperatures.

In the same line, ER stress was previously reported to induce Maf1-dependant repression of tRNA synthesis [64]. Accordingly, a significant reduction of pre-tRNA Leu was observed upon 4H Tm treatment in wild-type cells [Supplementary Fig. S5D, pre-tRNA(Leu) relative to untreated], while under the same treatment, cells inactivated for the RNA Polymerase III repressor Maf1 or Rrp6 showed significant accumulation of pre-tRNA-LEU (Supplementary Fig. S5D). Notably, this Maf1-dependant repression of tRNA synthesis may explain the reduced pre-tRNA-LEU accumulation observed in *sen2-42* cells upon Tm treatment compared to untreated conditions (Figs. 5B and Supplementary Fig. S5A). Again, this accumulation of pre-tRNA was accompanied by increased resistance to Tm—that was less pronounced for *maf1*Δ cells than for *rrp6*Δ cells (Supplementary Fig. S5E)—and a significant reduction of the percentage of spliced *HAC1* in *rrp6*Δ and *maf1*Δ cells compared to WT cells (Supplementary Fig. S5F), reinforcing the possibility of causal relationship between pre-tRNA accumulation and reduced *HAC1* mRNA splicing.

As such, Trl1/Rlg1 OE (Supplementary Fig. S5G) slightly but consistently re-sensitized *rrp6*Δ cells to Tm (Supplementary Fig. S5H). However, the Tm sensitivity of *TRL1/RLG1* overexpressing *rrp6*Δ cells did not reach that of WT cells (Supplementary Fig. S5H, compare *rrp6*Δ+p$_{CUP}$*TRL1* to WT). This prompted us to test whether the activity of Ire1 was similarly impeded in *rrp6*Δ cells by the accumulation of unprocessed RNA species. Indeed, when Trl1/Rlg1 and Ire1 were co-overexpressed (Supplementary Fig. S5I), the sensitization of *rrp6*Δ to ER stress was now more pronounced (Fig. 5E), reaching that of WT cells co-overexpressing Trl1/Rlg1 and Ire1. Together, this indicates that the activity of Ire1, like Trl1/Rlg1, is hindered in *rrp6*Δ cells. In addition, analysis of *HAC1* mRNA splicing (Fig. 5F) revealed that co-overexpression of Ire1 and Trl1/Rlg1 increased *HAC1* splicing in both wild-type and *rrp6*Δ cells in the absence of ER stress. However, upon 4H Tm treatment, increased *HAC1* mRNA splicing was only observed in *rrp6*Δ cells, likely because splicing had already reached a maximum in wild-type cells and supporting that *HAC1* mRNA splicing is limited in *rrp6*Δ cells.

Finally, expressing an intron-less form of *HAC1* (*hac1*Δi) as the sole form of *HAC1* in WT and *rrp6*Δ cells resulted in opposite phenotypes: it increased the Tm resistance of WT cells while sensitizing *rrp6*Δ cells to ER stress (Fig. 5G). This indicates that when they express the same level of Hac1 (Supplementary Fig. S5J), *rrp6*Δ cells no longer have a growth advantage in the presence of ER stress and it further emphasizes the key influence of splicing lessening on *rrp6*Δ cells' ER stress resistance phenotype.

Collectively, these results support that limitation of UPR signaling, via a reduction of *HAC1* splicing mediated by an out-titration of its splicing machinery, is a central mechanism that allows *rrp6*Δ cells to better cope with ER stress than wild-type cells.

Rrp6 cooperates with Isw1 for accurate UPR deactivation

Previously, we demonstrated cooperation between the ribonucleolytic activity of Rrp6 and the mRNA nuclear retention activity of Isw1 for optimal quality control of mRNA biogenesis [65]. To investigate how their respective activities integrate to control the UPR duration, we analyzed the phenotype of *isw1*Δ *rrp6*Δ cells. Upon *RRP6* inactivation, *isw1*Δ cells, which are more sensitive to ER stress than WT (Fig. 6A and [12] became resistant to ER stress (Fig. 6A) and their kinetics of UPR termination was similar to that of *rrp6*Δ cells (Fig. 6B and Supplementary Fig. S6A). This epistatic relation indicates that the physiological consequences of excess cytoplasmic *HAC1* mRNA resulting from *ISW1* inactivation are overcome in the absence of *RRP6* through splicing inhibition. Conversely, limiting the nuclear export of the constitutively spliced form of *HAC1* mRNA (*hac1*Δi) by overexpressing *ISW1* [12] fostered the resistance of *rrp6*Δ *hac1*Δi cells to ER stress (Fig. 6C). Hence, the genetic alteration of the expression level of one of these two partners is sufficient to influence the UPR phenotype of cells inactivated for the other partner.

To investigate whether and how these factors shape the UPR in a wild-type context, we sought to analyze how ER stress influences their expression. We already reported that Isw1 is induced during the UPR, which provides a negative feedback loop, critical for accurate UPR abatement [12]. Conversely, the expression of *RRP6* was significantly decreased both at the mRNA and protein levels upon Tm treatment compared to untreated conditions (Supplementary Fig. S6B and C), as previously reported [31]. This decrease is consistent with the specific stabilization of Rrp6-sensitive transcripts upon ER stress (Supplementary Fig. S2B) and designates physiological downregulation of *RRP6* expression as part of the shutdown mechanism of UPR signaling. To assess the significance of this downregulation, we analyzed the stress sensitivity of cells expressing *RRP6* under the control of the promotor of a UPR gene with similar transcription under basal conditions [66], *PMI40,* to prevent its ER stress-induced downregulation. Expectedly, under basal conditions, the steady-state level of Rrp6 was comparable in cells expressing the chimeric construct and wild-type cells. In contrast, Tm treatment respectively induced a decrease and an increase in Rrp6 level in WT and mutant cells (Fig. 6D). Strikingly, impairment of the natural decline of Rrp6 expression upon ER stress led to a decreased resistance to Tm, even more pronounced than in WT cells (Fig. 6E, compare *rrp6*Δ+p$_{PMI40}$*RRP6* to *rrp6*Δ+p*RRP6*).

Altogether, our results bring to the fore RNA metabolism, namely RNA export, and degradation, as significant instructors of UPR duration (Fig. 6F). Limitation of *HAC1* mRNA cytoplasmic splicing is achieved through ER stress-mediated induction of Isw1, which restricts *HAC1* mRNA nuclear export, as well as through the inhibition of *HAC1* mRNA splicing machinery resulting from ER stress-induced Rrp6 downregulation.

Discussion

While the UPR serves a protective function toward defective ER proteostasis, the toxicity of prolonged or inappropriate UPR signaling is increasingly recognized, even in the absence of apoptotic induction [67]. Through meticulous analysis of the transcriptional UPR output in yeast cells inactivated for Rrp6 and Isw1, two actors of nuclear RNA quality control, our work reveals how seemingly modest variations in the level and duration of UPR activation can dramatically tip the balance between cell survival (this study) and cell death [12].

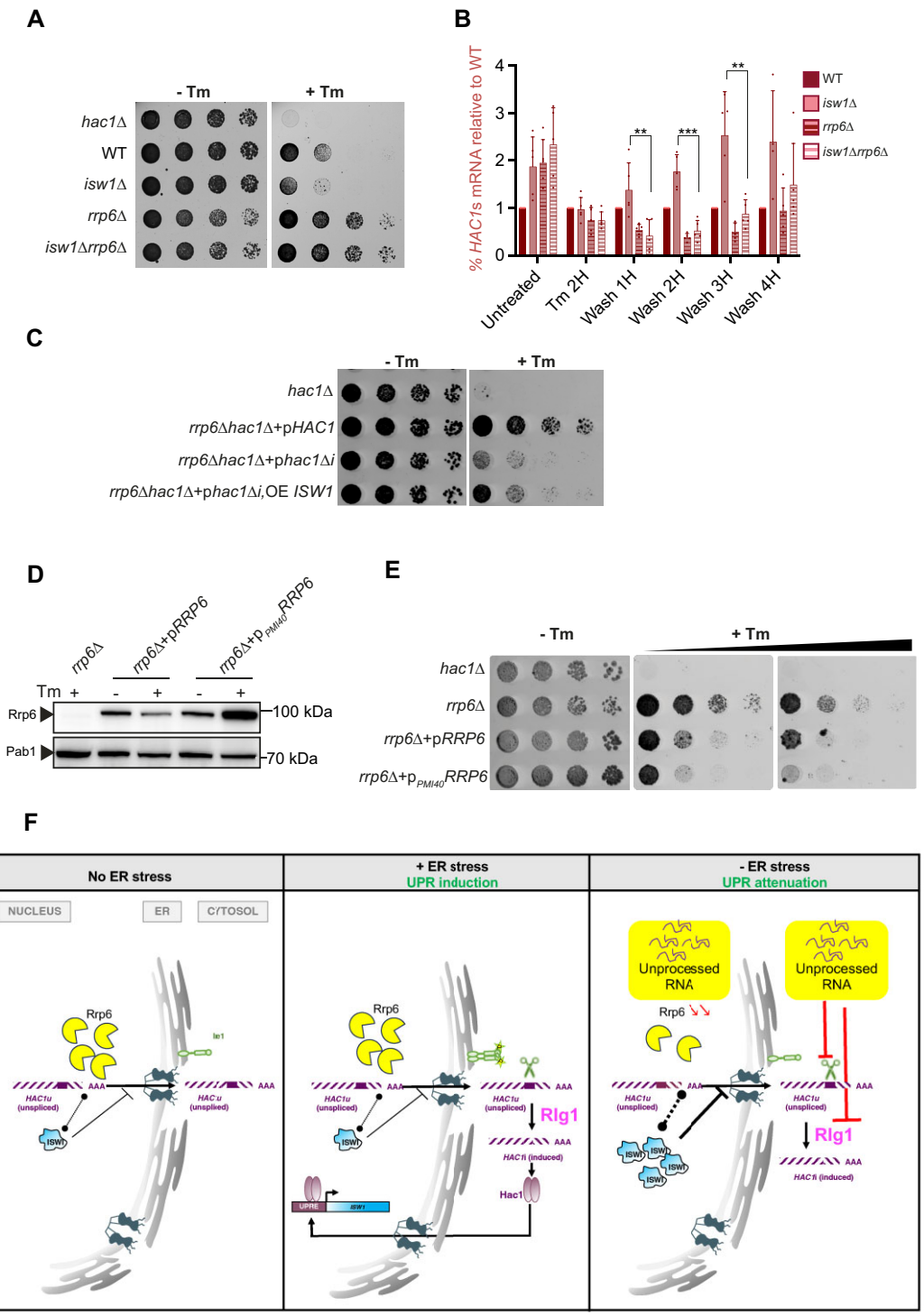

Figure 6. UPR termination is under control of the cooperative activity of Rrp6 and Isw1. (**A**) Five-fold serial dilutions of the indicated strains grown for 3 days at 30°C on YPD media containing (+Tm) or not (−Tm) 0.6 μg/ml Tm. (**B**) *HAC1* mRNA splicing was analyzed by RT-qPCR in WT, *isw1*Δ, *rrp6*Δ and *isw1*Δ *rrp6Δ* during the Tm UPR time-course depicted in Fig. 3A. $n = 5$ independent experiments, mean ± SD. Unpaired one-tail *t*-test (*P*-values *isw1*Δ *rrp6*Δ relative to *isw1*Δ: 1.61E-01, 6.73E-02, 5.87E-03, 8.21E-05, 2.45E-03 and 6.19E-02 for Untreated, Tm 2H, Wash 1H, Wash 2H, Wash 3H, Wash 4H, respectively). (**C**) OE of *ISW1* partially rescues the Tm sensitivity of *rrp6*Δ expressing the constitutively spliced form of *HAC1* (*hac1*Δi) as the only form of *HAC1*. Five-fold serial dilutions of the indicated strains grown for 3 days at 30°C on media containing (+Tm) or not (−Tm) 0,6 μg/ml Tm. (**D**) Rrp6 expression level upon promotor change. Total protein extracts from exponentially growing cells of the indicated genotype were analyzed by western blot with anti-Rrp6 and anti-Pab1 (loading) antibodies. (**E**) Preventing ER stress-mediated *RRP6* downregulation sensitizes stress to Tm. Five-fold serial dilutions of the indicated strains grown for 3 days at 30°C on media containing 0.6 μg/ml or 0.8 μg/ml Tm (+Tm) or not (−Tm). (**F**) Model: RNA metabolism instructs UPR duration. In the absence of ER stress Isw1 regulates the nuclear export of the *HAC1* mRNA whose steady state level is controlled by the exonuclease activity of Rrp6. ER stress turns on the UPR, which results in an induction of Isw1 expression that fosters *HAC1* mRNA nuclear retention [12]. In addition, this study reveals that ER stress-mediated down regulation of *RRP6* expression leads to the accumulation of unprocessed RNAs, which divert the activity of the *HAC1* mRNA splicing machinery. Together, these mRNA metabolism events significantly contribute to accurate UPR abatement, which is critical for cells' survival to ER stress.

Interestingly, although both *isw1*Δ and *rrp6*Δ cells show increased basal levels of the spliced form of *HAC1* compared to wild-type cells, they display opposite resistance to ER stress, indicating that basal active *HAC1* mRNA level is not the main driver of this phenotype. Our transcriptional analysis of the UPR kinetics unexpectedly revealed prolonged and shortened expression of *HAC1*s mRNA and Hac1 transcriptional targets for *isw1*Δ and *rrp6*Δ cells, respectively. While stabilization of *HAC1* mRNA in the absence of *RRP6* was previously proposed to boost up UPR activation and thus enhance *rrp6*Δ cells' resistance to ER stress [31], our results suggested that the mechanistic underpinning of this resistance remained incompletely understood and opened up the intriguing possibility that ER stress resistance could stem from the lowering of UPR signaling. Accordingly, artificial interruption of UPR signaling was sufficient to significantly increase cell viability upon ER stress (Fig. 4), and *sen2-42* cells, in which *HAC1*mRNA splicing is lessened, presented a marked resistance to ER stress (Fig. 5). Of note, while the level of *HAC1*s mRNA was reduced in both *rrp6*Δ and *sen2-42* cells upon ER stress, it varied in opposite directions relative to WT under basal conditions, indicating again that although significant, the variations of basal *HAC1*s levels in these mutants do not significantly contribute to cell fitness upon ER stress, which instead depends on the intensity and duration of UPR signaling [1].

Although the origin of yeast cell lethality upon ER stress is still uncertain, sustained UPR activation was proposed to overload the translocation machinery [11, 13], leading to the mislocalization of ER-resident proteins with crucial functions in ER homeostasis. Thus, time-course analysis of the glycosylation profile of Pdi1 after Tm treatment stands as a dedicated tool to analyze ER congestion. Pdi1 possesses five glycosylation sites and is translocated post-translationally into the ER lumen. Upon Tm wash, protein glycosylation can thus be monitored by western blot, on which discrete bands corresponding to the mono to penta-glycosylated forms of the protein are detected. Strikingly, while mutants impaired for UPR deactivation show delayed Pdi1 glycosylation profiles [12], the kinetics of Pdi1 glycosylation was enhanced in *rrp6*Δ cells compared to WT, indicating a faster recovery of ER homeostasis. This result is consistent with the reduced expression of UPR targets, among which genes encoding ER resident proteins are largely represented. Hence, a seemingly modest moderation of UPR signaling benefits cell fitness upon ER stress. Although a priori counterintuitive, this result is consistent with the transience of stress responses.

Mechanistically, we propose that inactivation of *RRP6* indirectly shapes the UPR through the titration of *HAC1* mRNA splicing machinery by unprocessed RNA species which, although not precisely characterized, are distinct from those generated upon Xrn1, Los1, or Nmd2 inactivation. Since Rrp6 is a nuclear exonuclease, the unprocessed RNA species resulting from its inactivation must primarily accumulate within the nucleus. This titration thus implies the export of these species to the cytoplasm, which is corroborated by previous studies reporting pre-mRNA cytoplasmic leakage upon *RRP6* inactivation [68, 69]. While Rrp6 and Trl1/Rlg1 share pre-tRNA as a common substrate, the nature of the RNA species that titrate Ire1 activity remains unclear given that *HAC1* mRNA is the only known Ire1 substrate in yeast [70] and therefore suggests a nonspecific titration. In line with this hypothesis, a set of RNAs—including mRNAs, rRNAs, and tRNAs—that directly interact with Ire1 and for which no evidence of Ire1-mediated cleavage could be detected, were identified in mammalian cells through photoactivable-ribonucleoside-crosslinking and immuno-precipitation approaches [71]. Finally, while the underlying mechanism responsible for ER stress-mediated *RRP6* down-regulation is currently unknown, similar expression dampening of *LRP1*, *TRF4,* and *DIS3* — genes whose inactivation confers resistance to ER stress (Fig. 1E and F) — has been reported [7, 72], evoking the possibility of a global ER stress-driven rewiring of these RNA decay factors.

Given that the cytoplasmic splicing of *HAC1* mRNA constitutes a molecular switch that triggers the UPR, the central contribution of RNA metabolism to UPR regulation comes with no surprise. Our data add another unsuspected layer of complexity to these regulations, whereby the ER stress-induced regulation of Rrp6 expression indirectly influences the critical deactivation phase of the UPR signaling. In light of the large number of genes labeled with the gene ontology term 'RNA catabolism' and whose deletion was associated with increased resistance to ER stress in genome-wide screens, a deeper investigation of their contribution to cells' adaptation to ER stress is worth considering. In particular, after individual validation of their ER stress resistance phenotype, it would be critical to investigate whether, like *rrp6*Δ, these mutants indirectly shape the UPR through perturbation of global RNA metabolism or whether they specifically target the metabolism of *HAC1* or other UPR targets transcripts. In a context where sustained UPR activation in malignant and immune cells of the tumor microenvironment was reported to facilitate malignant progression [73], therapeutic targeting of these conserved RNA metabolism pathways may thus constitute an attractive alternative or complement customary UPR modulators.

Acknowledgements

We wish to thank Madhusudan Dey, Anita Hopper, Torben Heick Jensen, Domenico Libri, Odil Porrua, Nouhou Haidara, Tohru Yoshihisa, and Peter Walter for generous reagents sharing. We are grateful to Benoît Palancade for critical reading of the manuscript as well as all members of the Palancade lab for stimulating discussions.

Supplementary data

Supplementary data is available at NAR online.

Conflict of interest

None declared.

Funding

This work was supported by the Agence Nationale pour la Recherche (ANR-JC, grant 17-CE12-0023-01), the program "Investissement d'Avenir" launched by the French Government and implemented by ANR, with the reference "ANR-18-IdEx-0001" as part of its program "Emergence", the Fondation ARC pour la Recherche sur le Cancer (PJA20181207794 to AB) and the Ligue Contre le Cancer (RS19/75-45). Funding to pay the Open Access publication charges for this article was provided by ANR -18-IdEx-0001.

Data availability

Unique biological material generated in this study is available from the corresponding author upon reasonable request. Source data for each figure are provided with this paper as a source data file. Gene expression data have been deposited in ArrayExpress under accession codes E-MTAB-10511 and E-MTAB-13744.

References

1. Walter P, Ron D. The unfolded protein response: from stress pathway to homeostatic regulation. *Nat Rev Cancer* 2011;**334**:71–88.
2. Aragón T, van Anken E, Pincus D *et al.* Messenger RNA targeting to endoplasmic reticulum stress signalling sites. *Nature* 2009;**457**:736–40. https://doi.org/10.1038/nature07641
3. Sidrauski C, Cox JS, Walter P. tRNA ligase is required for regulated mRNA splicing in the unfolded protein response. *Cell* 1996;**87**:405–13. https://doi.org/10.1016/S0092-8674(00)81361-6
4. Di Santo R, Aboulhouda S, Weinberg DE. The fail-safe mechanism of post-transcriptional silencing of unspliced HAC1 mRNA. *eLife* 2016;**5**:e20069. https://doi.org/10.7554/elife.
5. Cox JS, Walter P. A novel mechanism for regulating activity of a transcription factor that controls the unfolded protein response. *Cell* 1996;**87**:391–404. https://doi.org/10.1016/S0092-8674(00)81360-4
6. Rüegsegger U, Leber JH, Walter P. Block of HAC1 mRNA translation by long-range base pairing is released by cytoplasmic splicing upon induction of the unfolded protein response. *Cell* 2001;**107**:103–14. https://doi.org/10.1016/S0092-8674(01)00505-0
7. Travers KJ, Patil CK, Wodicka L *et al.* Functional and genomic analyses reveal an essential coordination between the unfolded protein response and ER-associated degradation. *Cell* 2000;**101**:249–58. https://doi.org/10.1016/S0092-8674(00)80835-1
8. Chawla A, Chakrabarti S, Ghosh G *et al.* Attenuation of yeast UPR is essential for survival and is mediated by IRE1 kinase. *J Cell Biol* 2011;**193**:41–50. https://doi.org/10.1083/jcb.201008071
9. Lin JH, Li H, Yasumura D *et al.* IRE1 signaling affects cell fate during the unfolded protein response. *Science* 2007;**318**:944–9. https://doi.org/10.1126/science.1146361
10. Hetz C, Papa FR. The unfolded protein response and cell fate control. *Mol Cell* 2018;**69**:169–81. https://doi.org/10.1016/j.molcel.2017.06.017
11. Rubio C, Pincus D, Korennykh A *et al.* Homeostatic adaptation to endoplasmic reticulum stress depends on Ire1 kinase activity. *J Cell Biol* 2011;**193**:171–84. https://doi.org/10.1083/jcb.201007077
12. Matabishi-Bibi L, Challal D, Barucco M *et al.* Termination of the unfolded protein response is guided by ER stress-induced HAC1 mRNA nuclear retention. *Nat Commun* 2022;**13**:6331. https://doi.org/10.1038/s41467-022-34133-8
13. Schmidt RM, Schessner JP, Borner GHH *et al.* The proteasome biogenesis regulator Rpn4 cooperates with the unfolded protein response to promote ER stress resistance. *eLife* 2019;**8**:e43244. https://doi.org/10.7554/eLife.43244
14. Peffer S, Gonçalves D, Morano KA. Regulation of the Hsf1-dependent transcriptome via conserved bipartite contacts with Hsp70 promotes survival in yeast. *J Biol Chem* 2019;**294**:12191–202. https://doi.org/10.1074/jbc.RA119.008822
15. Krakowiak J, Zheng X, Patel N *et al.* Hsf1 and Hsp70 constitute a two-component feedback loop that regulates the yeast heat shock response. *eLife* 2018:**7** :e31668.
16. Soo SK, Traa A, Rudich PD *et al.* Activation of mitochondrial unfolded protein response protects against multiple exogenous stressors. *Life Sci Alliance* 2021;**4**:e202101182. https://doi.org/10.26508/lsa.202101182
17. Pincus D, Chevalier MW, Aragón T *et al.* BiP binding to the ER-stress sensor Ire1 tunes the homeostatic behavior of the unfolded protein response. *PLoS Biol* 2010;**8**:e1000415. https://doi.org/10.1371/journal.pbio.1000415
18. Guo J, Polymenis M. Dcr2 targets Ire1 and downregulates the unfolded protein response in *Saccharomyces cerevisiae*. *EMBO Rep* 2006;**7**:1124–7. https://doi.org/10.1038/sj.embor.7400813
19. Eletto D, Eletto D, Dersh D *et al.* Protein disulfide isomerase A6 controls the decay of IRE1α signaling via disulfide-dependent association. *Mol Cell* 2014;**53**:562–76. https://doi.org/10.1016/j.molcel.2014.01.004
20. Li X, Sun S, Appathurai S *et al.* A molecular mechanism for turning off IRE1α signaling during endoplasmic reticulum stress. *Cell Rep* 2020;**33**:108563. https://doi.org/10.1016/j.celrep.2020.108563
21. Lisbona F, Rojas-Rivera D, Thielen P *et al.* BAX inhibitor-1 is a negative regulator of the ER stress sensor IRE1alpha. *Mol Cell* 2009;**33**:679–91. https://doi.org/10.1016/j.molcel.2009.02.017
22. Karam R, Lou CH, Kroeger H *et al.* The unfolded protein response is shaped by the NMD pathway. *EMBO Rep* 2015;**16**:599–609. https://doi.org/10.15252/embr.201439696
23. Prajapati HK, Ocampo J, Clark DJ. Interplay among atp-dependent chromatin remodelers determines chromatin organisation in yeast. *Biology (Basel)* 2020;**9**:190.
24. Dargemont C, Babour A. Novel functions for chromatin dynamics in mRNA biogenesis beyond transcription. *Nucleus* 2017;**8**:482–488. https://doi.org/10.1080/19491034.2017.1342916
25. Babour A, Shen Q, Dos-Santos J *et al.* The chromatin remodeler ISW1 is a quality control factor that surveys nuclear mRNP biogenesis. *Cell* 2016;**167**:1201–14. https://doi.org/10.1016/j.cell.2016.10.048
26. Fox MJ, Mosley AL. Rrp6: integrated roles in nuclear RNA metabolism and transcription termination. *Wiley Interdiscip Rev RNA* 2016;**7**:91–104. https://doi.org/10.1002/wrna.1317
27. Mitchell P, Petfalski E, Shevchenko A *et al.* The exosome: a conserved eukaryotic RNA processing complex containing multiple 3'→5' exoribonucleases. *Cell* 1997;**91**:457–66. https://doi.org/10.1016/S0092-8674(00)80432-8
28. Schneider C, Kudla G, Wlotzka W *et al.* Transcriptome-wide analysis of exosome targets. *Mol Cell* 2012;**48**:422–33. https://doi.org/10.1016/j.molcel.2012.08.013
29. Gudipati RK, Xu Z, Lebreton A *et al.* Extensive degradation of RNA precursors by the exosome in wild-type cells. *Mol Cell* 2012;**48**:409–21. https://doi.org/10.1016/j.molcel.2012.08.018
30. Kapitzky L, Beltrao P, Berens TJ *et al.* Cross-species chemogenomic profiling reveals evolutionarily conserved drug mode of action. *Mol Syst Biol* 2010;**6**:451. https://doi.org/10.1038/msb.2010.107
31. Sarkar D, Paira S, Das B. Nuclear mRNA degradation tunes the gain of the unfolded protein response in *Saccharomyces cerevisiae*. *Nucleic Acids Res* 2018;**46**:1139–56. https://doi.org/10.1093/nar/gkx1160
32. Longtine MS, McKenzie A, Demarini DJ *et al.* Additional modules for versatile and economical PCR-based gene deletion and modification in *Saccharomyces cerevisiae*. *Yeast* 1998;**14**:953–61. https://doi.org/10.1002/(SICI)1097-0061(199807)14:10(953::AID-YEA293)3.0.CO;2-U
33. Nishimura K, Fukagawa T, Takisawa H *et al.* An auxin-based degron system for the rapid depletion of proteins in nonplant cells. *Nat Methods* 2009;**6**:917–22. https://doi.org/10.1038/nmeth.1401
34. Cox JS, Shamu CE, Walter P. Transcriptional induction of genes encoding endoplasmic reticulum resident proteins requires a transmembrane protein kinase. *Cell* 1993;**73**:1197–206. https://doi.org/10.1016/0092-8674(93)90648-A
35. Burkard KTD, Butler JS. A nuclear 3′–5′ exonuclease involved in mRNA degradation interacts with poly(A) polymerase and the hnRNA protein Npl3p. *Mol Cell Biol* 2000;**20**:604. https://doi.org/10.1128/MCB.20.2.604-616.2000

36. Assenholt J, Mouaikel J, Andersen KR *et al.* Exonucleolysis is required for nuclear mRNA quality control in yeast THO mutants. *RNA* 2008;**14**:2305. https://doi.org/10.1261/rna.1108008
37. Silverstein RA, De Valdivia EG, Visa N. The incorporation of 5-fluorouracil into RNA affects the ribonucleolytic activity of the exosome subunit Rrp6. *Mol Cancer Res* 2011;**9**:332–40. https://doi.org/10.1158/1541-7786.MCR-10-0084
38. Fang F, Hoskins J, Butler JS. 5-Fluorouracil enhances exosome-dependent accumulation of polyadenylated rRNAs. *Mol Cell Biol* 2004;**24**:10766. https://doi.org/10.1128/MCB.24.24.10766-10776.2004
39. Feigenbutz M, Garland W, Turner M *et al.* The exosome cofactor Rrp47 is critical for the stability and normal expression of its associated exoribonuclease Rrp6 in *Saccharomyces cerevisiae*. *PLoS One* 2013;**8**:e80752. https://doi.org/10.1371/journal.pone.0080752
40. Stead JA, Costello JL, Livingstone MJ *et al.* The PMC2NT domain of the catalytic exosome subunit Rrp6p provides the interface for binding with its cofactor Rrp47p, a nucleic acid-binding protein. *Nucleic Acids Res* 2007;**35**:5556–67. https://doi.org/10.1093/nar/gkm614
41. Schmid M, Jensen TH. The nuclear RNA exosome and its cofactors. *Adv Exp Med Biol* 2019;**1203**:113–32. https://doi.org/10.1007/978-3-030-31434-7_4
42. Houseley J, Tollervey D. The nuclear RNA surveillance machinery: the link between ncRNAs and genome structure in budding yeast? *Biochim Biophys Acta* 2008;**1779**:239–46. https://doi.org/10.1016/j.bbagrm.2007.12.008
43. Lebreton A, Tomecki R, Dziembowski A *et al.* Endonucleolytic RNA cleavage by a eukaryotic exosome. *Nature* 2008;**456**:993–6. https://doi.org/10.1038/nature07480
44. Gudipati RK, Xu Z, Lebreton A *et al.* Extensive degradation of RNA precursors by the exosome in wild type cells. *Mol Cell* 2012;**48**:409. https://doi.org/10.1016/j.molcel.2012.08.018
45. Lecointe F, Simos G, Sauer A *et al.* Characterization of yeast protein Deg1 as pseudouridine synthase (Pus3) catalyzing the formation of Ψ38 and Ψ39 in tRNA anticodon loop. *J Biol Chem* 1998;**273**:1316–23. https://doi.org/10.1074/jbc.273.3.1316
46. Phizicky EM, Hopper AK. The life and times of a tRNA. *RNA* 2023;**29**:898–957. https://doi.org/10.1261/rna.079620.123
47. He F, Jacobson A. Identification of a novel component of the nonsense-mediated mRNA decay pathway by use of an interacting protein screen. *Genes Dev* 1995;**9**:437–54. https://doi.org/10.1101/gad.9.4.437
48. Larimer FW, Stevens A. Disruption of the gene XRN1, coding for a 5'—3' exoribonuclease, restricts yeast cell growth. *Gene* 1990;**95**:85–90. https://doi.org/10.1016/0378-1119(90)90417-P
49. Zanchin NIT, Goldfarb DS. The exosome subunit Rrp43p is required for the efficient maturation of 5.8S, 18S and 25S rRNA. *Nucleic Acids Res* 1999;**27**:1283–8. https://doi.org/10.1093/nar/27.5.1283
50. Allmang C, Mitchell P, Petfalski E *et al.* Degradation of ribosomal RNA precursors by the exosome. *Nucleic Acids Res* 2000;**28**:1684–91. https://doi.org/10.1093/nar/28.8.1684
51. Steffen KK, McCormick MA, Pham KM *et al.* Ribosome deficiency protects against ER stress in *Saccharomyces cerevisiae*. *Genetics* 2012;**191**:107–18. https://doi.org/10.1534/genetics.111.136549
52. Kuai L, Das B, Sherman F. A nuclear degradation pathway controls the abundance of normal mRNAs in *Saccharomyces cerevisiae*. *Proc Natl Acad Sci USA* 2005;**102**:13962–7. https://doi.org/10.1073/pnas.0506518102
53. Fox MJ, Gao H, Smith-Kinnaman WR *et al.* The exosome component Rrp6 is required for RNA polymerase II termination at specific targets of the Nrd1-Nab3 pathway. *PLoS Genet* 2015;**11**:e1004999. https://doi.org/10.1371/journal.pgen.1004999
54. Bicknell AA, Babour A, Federovitch CM *et al.* A novel role in cytokinesis reveals a housekeeping function for the unfolded protein response. *J Cell Biol* 2007;**177**:1017–27. https://doi.org/10.1083/jcb.200702101
55. Li J, Wang JJ, Zhang SX. Preconditioning with endoplasmic reticulum stress mitigates retinal endothelial inflammation via activation of X-box binding protein 1. *J Biol Chem* 2011;**286**:4912–21. https://doi.org/10.1074/jbc.M110.199729
56. Mendes CS, Levet C, Chatelain G *et al.* ER stress protects from retinal degeneration. *EMBO J* 2009;**28**:1296–307. https://doi.org/10.1038/emboj.2009.76
57. Kozlowski L, Garvis S, Bedet C *et al.* The *Caenorhabditis elegans* HP1 family protein HPL-2 maintains ER homeostasis through the UPR and hormesis. *Proc Natl Acad Sci USA* 2014;**111**:5956–61. https://doi.org/10.1073/pnas.1321698111
58. Brown RE, Su XA, Fair S *et al.* The RNA export and RNA decay complexes THO and TRAMP prevent transcription-replication conflicts, DNA breaks, and CAG repeat contractions. *PLoS Biol* 2022;**20**:e3001940. https://doi.org/10.1371/journal.pbio.3001940
59. Castelnuovo M, Rahman S, Guffanti E *et al.* Bimodal expression of PHO84 is modulated by early termination of antisense transcription. *Nat Struct Mol Biol* 2013;**20**:851–8. https://doi.org/10.1038/nsmb.2598
60. Villa T, Barucco M, Martin-Niclos MJ *et al.* Degradation of non-coding RNAs promotes recycling of termination factors at sites of transcription. *Cell Rep* 2020;**32**:107942. https://doi.org/10.1016/j.celrep.2020.107942
61. Moreau K, Le Dantec A, Mosrin-Huaman C *et al.* Perturbation of mRNP biogenesis reveals a dynamic landscape of the Rrp6-dependent surveillance machinery trafficking along the yeast genome. *RNA Biol* 2019;**16**:879. https://doi.org/10.1080/15476286.2019.1593745
62. Dhungel N, Hopper AK. Beyond tRNA cleavage: novel essential function for yeast tRNA splicing endonuclease unrelated to tRNA processing. *Genes Dev* 2012;**26**:503–14. https://doi.org/10.1101/gad.183004.111
63. Yoshihisa T, Ohshima C, Yunoki-Esaki K *et al.* Cytoplasmic splicing of tRNA in *Saccharomyces cerevisiae*. *Genes Cells* 2007;**12**:285–97. https://doi.org/10.1111/j.1365-2443.2007.01056.x
64. Upadhya R, Lee JH, Willis IM. Maf1 Is an essential mediator of diverse signals that repress RNA polymerase III transcription. *Mol Cell* 2002;**10**:1489–94. https://doi.org/10.1016/S1097-2765(02)00787-6
65. Babour A, Shen Q, Dos-Santos J *et al.* The chromatin remodeler ISW1 is a quality control factor that surveys nuclear mRNP biogenesis. *Cell* 2016;**167**:1201–14. https://doi.org/10.1016/j.cell.2016.10.048
66. Pelechano V, Chávez S, Pérez-Ortín JE. A complete set of nascent transcription rates for yeast genes. *PLoS One* 2010;**5**:e15442. https://doi.org/10.1371/journal.pone.0015442
67. Tabas I, Ron D. Integrating the mechanisms of apoptosis induced by endoplasmic reticulum stress. *Nat Cell Biol* 2011;**13**:184–90. https://doi.org/10.1038/ncb0311-184
68. Sorenson MR, Stevens SW. Rapid identification of mRNA processing defects with a novel single-cell yeast reporter. *RNA* 2014;**20**:732. https://doi.org/10.1261/rna.042663.113
69. Galy V, Gadal O, Fromont-Racine M *et al.* Nuclear retention of unspliced mRNAs in yeast is mediated by perinuclear Mlp1. *Cell* 2004;**116**:63–73. https://doi.org/10.1016/S0092-8674(03)01026-2
70. Niwa M, Patil CK, DeRisi J *et al.* Genome-scale approaches for discovering novel nonconventional splicing substrates of the Ire1 nuclease. *Genome Biol* 2005;**6**:R3.
71. Acosta-Alvear D, Karagöz GE, Fröhlich F *et al.* The unfolded protein response and endoplasmic reticulum protein targeting machineries converge on the stress sensor IRE1. *eLife*2018;**7**:e43036. https://doi.org/10.7554/eLife.43036
72. Gasch AP, Spellman PT, Kao CM *et al.* Genomic expression programs in the response of yeast cells to environmental changes. *Mol Biol Cell* 2000;**11**:4241–57. https://doi.org/10.1091/mbc.11.12.4241

73. Chen X, Cubillos-Ruiz JR. Endoplasmic reticulum stress signals in the tumour and its microenvironment. *Nat Rev Cancer* 2021;**21**:71. https://doi.org/10.1038/s41568-020-00312-2

74. Morawska M, Ulrich HD. An expanded tool kit for the auxin-inducible degron system in budding yeast. *Yeast* 2013;**30**:341–51. https://doi.org/10.1002/yea.2967

Received: October 31, 2024. **Revised:** January 27, 2025. **Editorial Decision:** January 29, 2025. **Accepted:** February 3, 2025